

TALLINN UNIVERSITY OF TECHNOLOGY

Faculty of Science

Institute of Cybernetics

**Formation and detection of hidden solitons in
the hierarchical Korteweg-de Vries system**

MSc thesis

Martin Lints

Supervisor: Professor Andrus Salupere

Engineering physics

2013

I hereby declare that this work is a result of my original investigation. It has not been previously submitted for any academic degree. I affirm that all opinions, problem statements, collected data, etc. of other authors are cited properly.

Martin Lints

Supervisor: Professor Andrus Salupere

This work fulfills all the requirements of a masters thesis

Head of the defense committee:

Allowed for thesis defense

.....

(name, signature, date)

TALLINNA TEHNIKAÜLIKOOL

Matemaatika-loodusteaduskond

Küberneetika Instituut

**Peidetud solitonide formeerumine ja
tuvastamine hierarhilises Kortewegi-de Vriesi
süsteemis**

Magistritöö

Martin Lints

Juhendaja: Professor Andrus Salupere

Tehniline füüsika

2013

Contents

Introduction	5
1 Hidden solitons	7
2 Model equation	8
3 Initial conditions	9
3.1 Cnoidal wave	9
3.2 Harmonic wave	11
3.3 Sech ² -type solitary wave	12
3.4 Lengthened cn^2 wave	12
3.5 Initial waves	13
4 Numerical method	14
4.1 The essence of Fourier collocation method	14
4.2 Modification of the pseudospectral method for the model equation	16
5 Instabilities and filtering	17
5.1 Lower limit on the number of space grid points	17
5.2 Upper limit on the number of space grid points	19
5.3 Filtering	20
5.4 Shape of the initial profile	20
5.5 Conserved quantities	21
6 Analysis tools and methods	22
6.1 Direct tools	22
6.1.1 Pseudocolor plot	22
6.1.2 Wave profile maxima curves	23
6.2 Discrete Spectral Analysis	25
6.2.1 Spectral amplitudes and spectral densities	25
6.2.2 Cumulative spectrum and time averaged normalised spectral densities	26
6.3 Spectral detection of hidden solitons	27
6.4 Parameter space	29

7	Results and discussion	32
7.1	The influence of the initial wave on the results	32
7.1.1	The emergence of hidden solitons and tail	34
7.1.2	The concurrency of the interactions with the spectral amplitude peaks	36
7.1.3	The concurrency of t_k moments with the interactions	40
7.2	The influence of the microstructural dispersion parameter α_2	43
7.3	The influence of the change of the macrostructural dispersion parameter α_1 and amplitude A	44
	Conclusions	47
	Resümee	50
	Acknowledgments	51
A	Example: FFT of $\sin(x)$ where $x \in [0, 2\pi)$	54

Introduction

In 1895, Korteweg and de Vries published their celebrated paper [1] on the propagation of nonlinear long waves in shallow water. From these beginnings has evolved the physics of solitons: a very broad field under active development, encompassing the hydrodynamic waves, plasma waves, the propagation of information in transmission lines and optical cables and the propagation of waves in granular materials.

Because in this thesis the model equation is not Korteweg-de Vries (KdV) and is non-integrable, “soliton” is here defined to be any solitonic structure which behaves as a soliton (i.e. is stable, interacts elastically and does not lose amplitude, propagates with a constant speed and amplitude).

Solitons can have some interesting properties, like the emergence of hidden solitons, introduced by Salupere et al. for Korteweg-de Vries (KdV) equation with harmonic initial wave [2]. These hidden (or virtual) solitons do not emerge in the initial train of solitons and can be detected in short time intervals only, usually after some interactions. The hidden solitons can, however, carry enough energy to affect the resulting solution by interacting with other solitons. For perturbed KdV, Salupere and Engelbrecht [3] show that hidden solitons can be amplified and carry substantial energy. The importance and motivation for this thesis comes from the large potential influence of these hidden solitons on the result.

Wave propagation in dilatant granular materials can be modelled by hierarchical Korteweg-de Vries (HKdV) equation derived by Giovine and Oliveri [4]. A material is dilatant if the deformation of the continuum introduces the expansion of voidage between the microstructure. The properties of the solutions emerging from asymptotic initial waves in HKdV has previously been investigated by Ilison [5]. His results are used for finding the right parameter space for the analysis at hand.

In this thesis the HKdV equation is solved numerically as an initial value problem using the cnoidal initial wave. This is a novelty, usually in this kind of analysis the harmonic or sech^2 -shaped IC is used. The cnoidal wave was initially studied by Korteweg and de Vries [1], but the concept has seen little attention since. In this thesis the cnoidal waves are used as a basis for the initial condition (IC) of the model equation. They allow arbitrary spatial period length and various shapes of the initial condition while being

smooth and in good agreement with the model equation. Only numerical methods are used because the model equation is non-integrable. The equation is integrated using pseudospectral methods and the solution is analysed by Discrete Spectral Analysis (DSA) as introduced by Salupere [6].

The main goals of the present thesis are:

- Solving the HKdV equation numerically over a wide range of material and IC parameters, under ICs of:
 - cnoidal wave;
 - “lengthened” Jacobi cn^2 -shaped wave;
 - sech^2 -shaped wave.
- Analysing the solution with discrete spectral analysis in order to characterise the soliton emergence process in terms of the Fourier spectrum.
- Characterising the influence of the equation parameters, and the initial condition type and parameters on the formation and detection of hidden solitons.

This thesis is divided as follows: Section 1 introduces the concept of hidden solitons; in Section 2 the model equation will be introduced; in Section 3 various initial conditions are discussed under which the model equation is numerically solved; the solving method and its numerical properties are discussed in Sections 4 and 5; the analysis methods are introduced in Section 6; the main results are summarised, analysed and discussed in Section 7. The scope of this thesis included writing the solvers and analysis software and calculating the results.

The preliminary results of this study have been presented in IMACS International Conference [7].

1 Hidden solitons

Hidden (or virtual) solitons were introduced by Salupere et al. [2, 3, 6, 8]. It was found that some small solitons are not visible in the initial soliton train [2]. Their influence on the larger solitons could be detected and they can become visible after some time and interactions.

In [8] the solution of KdV from initial sinusoidal wave is analysed using DSA. It was found that the actual number of emerging solitons is larger than can be seen from initial wave train or estimated from inverse scattering theorem. Additionally, it was shown that the DSA could also be used to estimate the interactions. Salupere [6] explains and gives an example of how the amplitude changes of visible solitons and spectral characteristics can be used to identify the number of visible and hidden solitons in the system.

Salupere and Engelbrecht [3] list the properties of the hidden solitons:

- They “can emerge from harmonic excitations and have the same physical background as visible solitons.”
- They “can be detected in wave profiles for a short time interval only when several soliton interactions have taken place and the reference state is fluctuating.”
- They “cause changes, specific to the soliton-type interaction, in the amplitudes and trajectories of the other solitons interacting with them.”

It is also said that the hidden solitons can capture energy and in non-conservative cases can become visible [3].

Hidden solitons in KdV systems have also been analysed by Christov [9] using the periodic inverse scattering theorem. In addition to the soliton modes, the spectrum of emerged modes was found to also contain “...less nonlinear oscillation modes, e.g., nonlinearly interacting cnoidal waves...”. However, this (periodic inverse scattering theorem) analysis requires the equation to be integrable, making it unsuitable for the problem at hand.

2 Model equation

Wave propagation in dilatant granular materials can be modelled by HKdV equation, derived by Giovine and Oliveri [4]. Dilatancy is the expansion of voidage in tightly packed granular arrangement when subjected to deformation [5]. An example of dilatant granular material is packed sand in a watery environment. On deformation the water does not extrude but seeps further into the material.

The model equation has some restrictive assumptions [4]:

- The case is conservative.
- The particles are elastic.
- The particles are surrounded by compressible fluid.
- Fluid density is negligible compared to density of particles.
- In a ball of radius ζ are no diffusion of grains nor any relative rotations (of grain, etc.).

The resulting equation governs the nonlinear wave motion near the equilibrium in dilatant materials:

$$\frac{\partial u}{\partial t} + u \frac{\partial u}{\partial x} + \alpha_1 \frac{\partial^3 u}{\partial x^3} + \beta \frac{\partial^2}{\partial x^2} \left(\frac{\partial u}{\partial t} + u \frac{\partial u}{\partial x} + \alpha_2 \frac{\partial^3 u}{\partial x^2} \right) = 0, \quad (1)$$

where

u is bulk density,

x is space coordinate,

t is time coordinate,

α_1 is macrostructure dispersion parameter,

α_2 is microstructure dispersion parameter,

β is microstructure parameter describing the ratio of grain size and wavelength.

The sign of β depends on the ratio of kinetic and potential energies and is positive for lower values of kinetic energy and negative with higher values [5].

3 Initial conditions

The HKdV equation incorporates two KdV operators, one governing micro- and the other macrostructure:

$$\psi_1 + \beta(\psi_2)_{xx} = 0, \quad (2)$$

Where the KdV operator can be given in form

$$\psi_k = u_t + uu_x + \alpha_k u_{xxx}, \quad k = 1, 2, \quad (3)$$

where α_k is the dispersion parameter.

The macrostructure is characterised by ψ_1 , therefore an initial wave which is an analytical solution to $\psi_1 = 0$ can be chosen. The sinusoidal and sech^2 -shaped initial pulses are most widely used. Between these is a cnoidal wave which is mainly used in this work.

3.1 Cnoidal wave

The derivation of cnoidal wave solution by Bhatnagar [10] is as follows. The uniform wave train is obtained by substituting $u = u(\xi)$, $\xi = x - ct$. This leads to

$$-cu_\xi + uu_\xi + du_{\xi\xi\xi} = 0.$$

which can be integrated twice to give

$$cu + \frac{u^2}{2} + du_{\xi\xi} + D_1 = 0 \quad \Big| \cdot u_\xi,$$

$$-\frac{1}{2}cu^2 + \frac{1}{6}u^3 + \frac{1}{2}du_\xi^2 + D_1u + D_2 = 0.$$

This cubic equation has zeros μ , ν and η and can be solved for $u(\xi)$

$$u(\xi) = \nu + (\mu - \nu)\text{cn}^2 \left[\xi \sqrt{\frac{\mu - \eta}{12 \cdot \alpha_1}}, \sqrt{m} \right], \quad (4)$$

and period of such wave curve is given as

$$P = 4 \cdot \sqrt{\frac{3\alpha_1}{\mu - \eta}} \cdot K(\sqrt{m}), \quad (5)$$

where

m is elliptic parameter, defined as $m = \frac{\mu - \nu}{\mu - \eta}$, in [11],

μ is the profile maximum,

ν is the profile minimum,

η is parameter uniting the profile expression (4) with the period expression (5),

K is Legendre's complete elliptic integral of the first kind.

In this study $\nu = 0$ so the initial cnoidal shape is given by

$$u(x) = A \cdot \text{cn}^2 \left[x \sqrt{\frac{A - \eta}{12 \cdot \alpha_1}}, \sqrt{m} \right], \quad (6)$$

where A stands for amplitude of the wave.

The cnoidal wave is more general than the harmonic or the sech^2 -shaped waves. Taking the elliptic parameter of a cnoidal wave $m = 0$ produces a harmonic wave. Taking $m = 1$ results in a sech^2 -shaped wave. Thus the parameter m can be thought to characterise the ‘‘solitariness’’ of the cnoidal wave (Fig. 1).

The influence of the shape of the cnoidal wave on the solution can be analysed. This shape is, however, restricted to being a solution to $\psi_1 = 0$. This means that the shape of the cnoidal wave in this work depends on the macrostructural dispersion parameter, period length, and amplitude and cannot be changed independently.

For numerical simulations the parameter η is not known in advance. It describes the shape of the wave and depends on the dispersion parameter. Knowing the desired period P , it is solved from Eq. (5) and then put into Eq. (6). To solve Eq. (5) for η it is necessary to find Legendre's complete elliptic integrals of the first and second kind. These can be computed with high precision using algorithms from [12].

Cnoidal waves with $m \rightarrow 0$ (harmonic wave) and $m \rightarrow 1$ (sech^2 -shaped wave) are both the solutions to the KdV $\psi_1 = 0$, so they can be used as initial waves to HKdV in the present study. In the spectral analysis, it must also be considered that the harmonic

wave $m \rightarrow 0$ is monochromatic with only the 1st harmonic being nonzero, conversely as the sech^2 -shaped wave $m \rightarrow 1$ has the most effect of overtones compared to the 1st harmonic and the cnoidal wave is in-between.

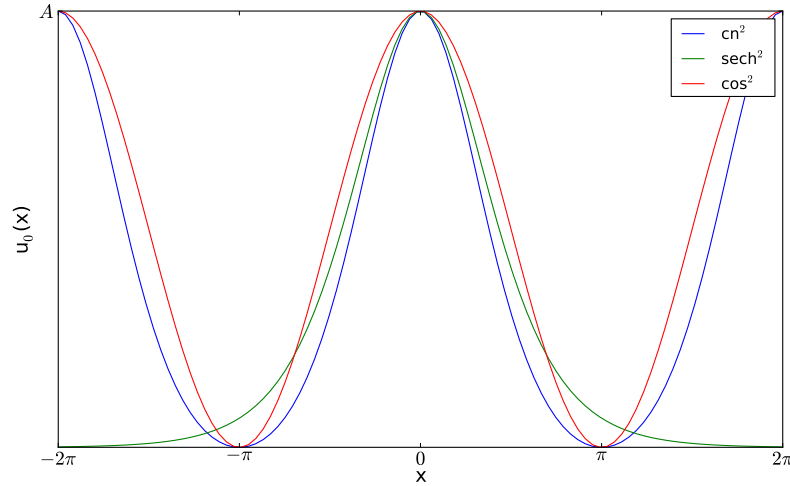


Figure 1: Different wave shapes

3.2 Harmonic wave

The harmonic IC can be considered a limiting case of cnoidal wave (6) where the elliptic parameter $m \rightarrow 0$ and thus the period $P \rightarrow 2\pi \cdot \sqrt{\frac{3\alpha_1}{A}}$ (Eq. (5)) but it is not easy to find parameters for cnoidal wave (6) which make it harmonic. A harmonic wave is smooth, very suitable for Fourier transform (lacking discontinuities) and DSA (the wave is monochromatic in $t = 0$) and usually produces a train of solitons. In addition, the harmonic wave is easy to generate and is intuitively interpreted. The famous Zabusky-Kruskal experiment [13] was done using it and the concept of hidden solitons was also discovered using the harmonic IC [2].

3.3 Sech²-type solitary wave

A sech²-shaped wave can be a true soliton for KdV equation, and is a limiting case of cnoidal wave (6) when the elliptic parameter $m \rightarrow 1$ and consequently the period tends to infinity $P \rightarrow \infty$. Its shape depends only on the dispersion parameter α_1 and amplitude A . The sech²-type solitary wave is a single bell-shaped hump given by

$$u(x) = A \cdot \operatorname{sech}^2 \left[x \sqrt{\frac{A}{12 \cdot \alpha_1}} \right], \quad (7)$$

moving without change in KdV system and decreasing asymptotically when $x \rightarrow \pm\infty$. Sech²-type initial pulse has gained widespread use in Centre for Nonlinear Studies in Institute of Cybernetics. It is mainly used for numerical analysis of microstructured nonlinear materials because it is stable and does not change under KdV, so any changes to soliton shape in propagation come from the effect of other complexities in the model studied. Unfortunately, because this IC is asymptotic, the spatial period needs to be quite long to avoid introducing discontinuities on the periodic boundary.

3.4 Lengthened cn² wave

Because the cnoidal wave profile touches the zero amplitude in finite distance, it is possible to cut out the cnoidal wave hump and pad it with zeros:

$$u(x) = \begin{cases} 0 & , & 0 \leq x < 3/2P \\ A \cdot \operatorname{cn}^2 \left[x \sqrt{\frac{A-\eta}{12 \cdot \alpha_1}}, \sqrt{m} \right] & , & 3/2P \leq x < 5/2P \\ 0 & , & 5/2P \leq x < 8/2P \end{cases} \quad (8)$$

The resulting profile will resemble the solitonic profile but the peak will be cnoidal wave (Fig. 2). The zero-padding will delay the influence of the periodic waves when compared to normal cnoidal profile. This kind of padding cannot generally be done with sech² profiles, because the period $P \rightarrow \infty$ there and inserting any zero-padding will generate discontinuities, as the sech² profile approaches the zero asymptotically, not in finite distance. It must be considered, however, that this lengthened cn² wave is no longer a solution to the $\psi_1 = 0$, unlike the cnoidal and sech²-shaped waves.

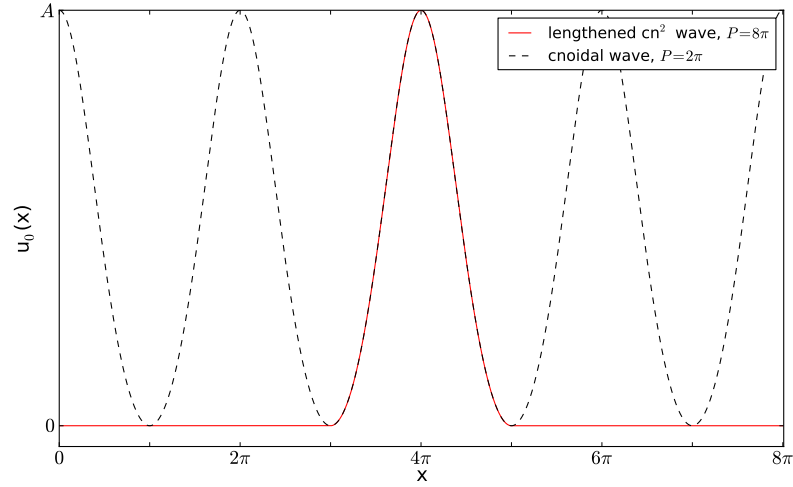


Figure 2: cn^2 initial waves

3.5 Initial waves

Three different initial waves are chosen for the analysis: (i) cnoidal wave ($P = 2\pi$) (6); (ii) lengthened cn^2 -shaped wave ($P = 8\pi$) (8); (iii) sech^2 -shaped wave ($P = 8\pi$) (7).

Cnoidal wave with $P = 2\pi$ should allow to generate hidden solitons. Because the boundary conditions are periodic, the emerging wave train will keep interacting with itself, hiding the small solitons behind large ones.

The lengthened cn^2 wave with period $P = 8\pi$ has the same peak shape as the cnoidal wave, but it is padded with zeros to allow the initial wave to decompose into a train of solitons before interactions begin. It is hoped that this will allow to see some solitons which are hidden in case of cnoidal initial wave.

The sech^2 -shaped initial wave also has the period $P = 8\pi$ and should also allow the decomposition of initial wave into a train of solitons before the interactions begin. Its shape is generally different from the cnoidal wave, thus it is not as comparable with the previous ICs. On the other hand, it is smoother than the lengthened cn^2 wave and can be chosen so the $\psi_1 = 0$ is satisfied, like the cnoidal wave.

4 Numerical method

The HKdV equation is solved using the pseudospectral (PS) collocation method. It means that the solution is approximated at gridpoints with a polynomial which is easy to differentiate. Unlike finite difference (FD) methods, this is a *global* method. Its main advantage is its low computational cost. Also, the pseudospectral method is very straightforward to use in case of nonlinearities and when the model includes high derivatives [14].

If restricted to equi-spaced grids on periodic domains and to problems that will not generate breaking waves or shock waves then the Fourier transform can be used to approximate the wave profile in space. The spatial derivatives are thus found by differentiating the spectrum of trigonometric functions and taking the inverse transform [6].

4.1 The essence of Fourier collocation method

A simple and very broadly applicable pseudospectral method is solving a PDE by first using Fast Fourier Transform (FFT) to calculate spatial derivatives and then advancing the solution in time using an ordinary differential equation (ODE) solver. This is also known as the method of lines [14].

If Discrete Fourier Transform (DFT) is defined by

$$U(k, t) = Fu = \sum_j^{N-1} u(j\Delta x, t) \exp\left(-\frac{2\pi i jk}{N}\right), \quad (9)$$

and inverse DFT (IDFT) by

$$u(j\Delta x, t) = F^{-1}U = \frac{1}{N} \sum_k U(k, t) \exp\left(\frac{2\pi i jk}{N}\right), \quad (10)$$

then differentiation $\frac{\partial}{\partial x}$ in original space transforms to multiplication by ik in Fourier space:

$$\frac{\partial^n u(x, t)}{\partial x^n} = F^{-1} [(ik)^n Fu].$$

Here

F is DFT operator,

F^{-1} is IDFT operator,

N is the number spatial grid points,

Δx is space grid length or space interval,

i is imaginary unit $i = \sqrt{-1}$,

k is wavenumber.

For the best speed performance in FFT algorithms, the number of spatial gridpoints should be a power of two: $N = \dots, 512, 1024, 2048, \dots$ etc. meaning N is even and wavenumbers are in the form

$$k = \left(-\frac{N}{2}\right), \left(-\frac{N}{2} + 1\right), \dots, -1, 0, 1, \dots, \left(\frac{N}{2} - 2\right), \left(\frac{N}{2} - 1\right). \quad (11)$$

In order to take the DFT of the wave profiles, the boundary condition must be periodic and the system must not generate breaking waves or shock waves.

In this work it is necessary to use a 2π -fold space period (as in $P = 2l\pi$ where $l = 1, 2, \dots$). As explained by Salupere [6], multiplication needs to be done with k/l instead of k when differentiating in case of $2l\pi$ space period:

$$\frac{\partial^n u(x, t)}{\partial x^n} = F^{-1} \left[\left(\frac{ik}{l} \right)^n F u \right]. \quad (12)$$

Also, the space grid range must not include the $2l\pi$ value: it must be in range $[0, 2l\pi)$, not $[0, 2l\pi]$. This is necessary for the periodic boundary conditions to be true.

For this work, the numerical codes were developed in Fortran, using FFTW library [15] for Fourier transforms and LSODE solver [16] for integration in time and wrapped to Python using f2py [17].

4.2 Modification of the pseudospectral method for the model equation

Since the HKdV equation contains a mixed partial derivative term βu_{xxt} , the equation has to be slightly modified to separate the derivatives for use with PS methods. The following is explained by Salupere in [6]: HKdV equation (1) is rewritten

$$(u + \beta u_{xx})_t + (u + 3\beta u_{xx}) u_x + (\alpha_1 + \beta u) u_{3x} + \beta \alpha_2 u_{5x} = 0$$

and variable $\phi = u + \beta u_{xx}$ is substituted in, expressing the time derivative

$$\phi_t = -(u + 3\beta u_{xx}) u_x - (\alpha_1 + \beta u) u_{3x} - \alpha_2 \beta u_{5x}$$

This equation can be integrated with ODE solvers if the variable u and its derivatives are expressed by

$$u = F^{-1} \left[\frac{F\phi}{1 - \beta k^2} \right], \quad \frac{\partial^n u}{\partial x^n} = F^{-1} \left[\frac{(ik)^n F\phi}{1 - \beta k^2} \right].$$

Therefore get the requirement for the value of β is that $1 - \beta k^2 \neq 0$.

5 Instabilities and filtering

The problem to be analysed is nonlinear and therefore susceptible to any numerical errors. The pseudospectral method has specific error sources which must be investigated. These sources will be discussed in this section and verification methods introduced.

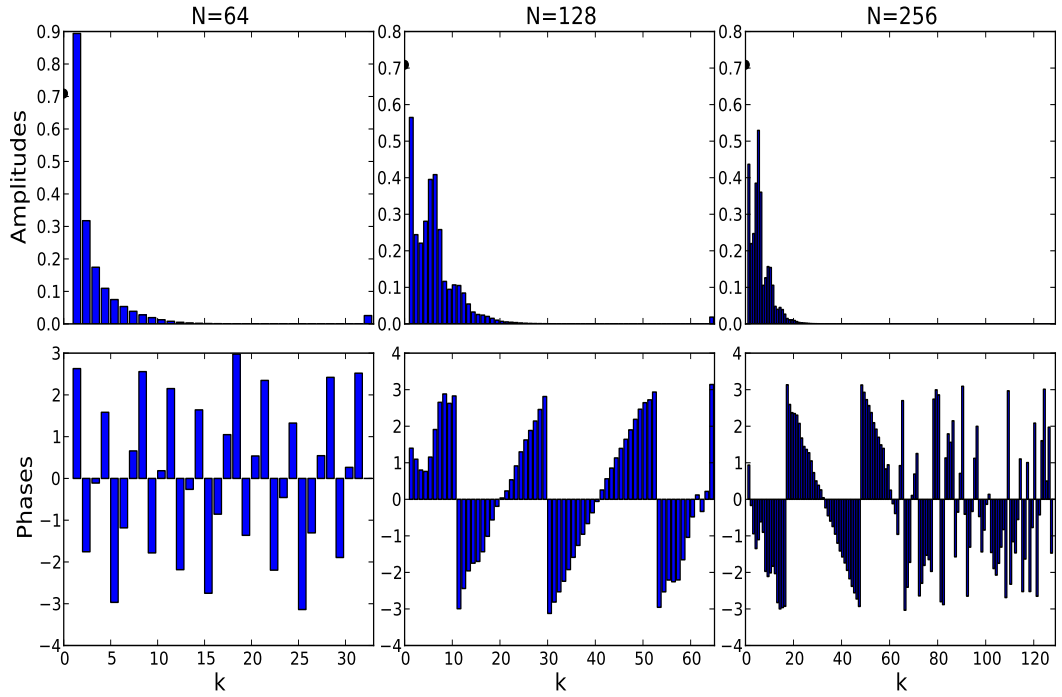
5.1 Lower limit on the number of space grid points

The data used for differentiating the wave profile is discrete, described only at nodes. This limits the amount of information or modes available from the Fourier transform. Therefore, in order to increase the precision, the grid must be refined, increasing the number of harmonic modes in the DFT spectrum.

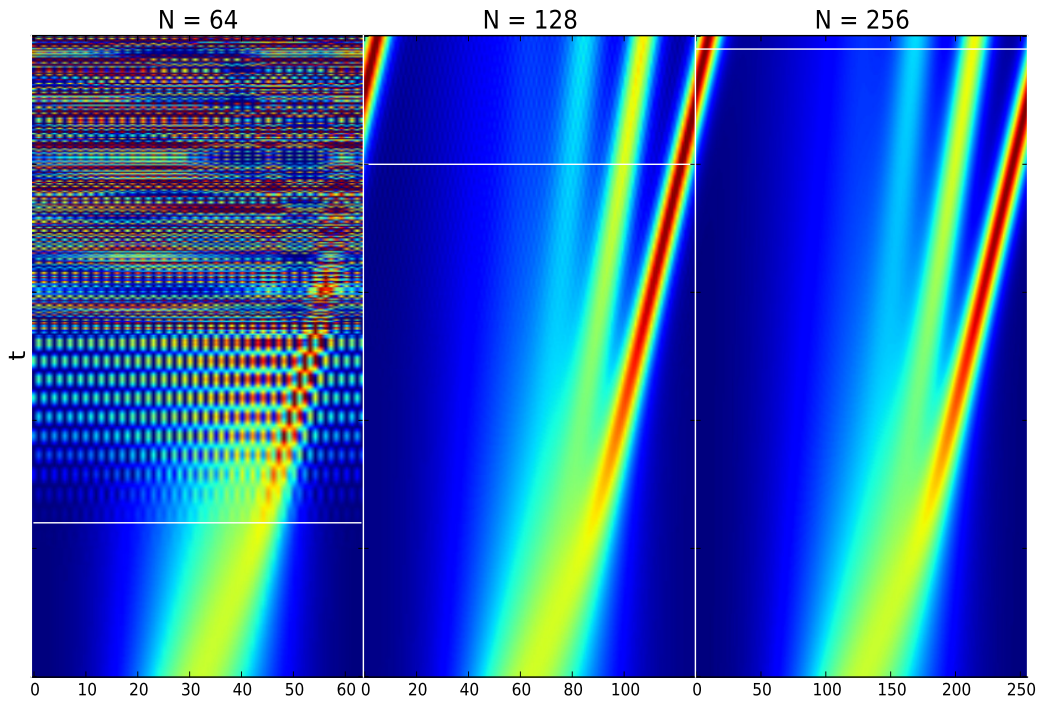
The problem that arises with too coarse space grid is that the high wavenumber modes are not represented and are, due to aliasing, misinterpreted as modes of lower wavenumbers. This might not be a problem for linear equations but, as mentioned by Fornberg [14, chapter 4.6], nonlinear terms multiply the frequencies: they bring energy to high wavenumbers, or alias it and produce errors.

For example, if $u(x) = \sin \alpha x$ then the KdV's nonlinear term $u(\partial u / \partial x) = (\alpha/2) \sin 2\alpha x$, doubling the frequency. If the number of gridpoints N is too small to contain all of the modes, then this high wavenumber information will be aliased to lower modes - most probably the highest mode that the spatial resolution N still allows (the Nyquist wavenumber). This is shown in Fig. 3(a): when $N = 64$, the mode $k = 32$ is filled and when $N = 128$ the mode $k = 64$ is filled. In this work, the Nyquist mode had been zeroed at every timestep to avoid collecting the aliased information. Any energy in this mode in Fig. 3(a) has emerged during just the last timestep.

These high frequency oscillations in case of $N = 64$ and $N = 128$ are also visible in Fig. 3(b). It appears as the solution had leaked some energy and regained it into the highest modes (Fig. 3(a)). This gives rise to oscillations which ultimately destroy the solution and is to be avoided. In case of $N = 256$, the highest mode is *not* filled and this resolution seems to be suitable. Therefore, if the grid is too coarse, the solution will become unstable and the coarser the grid, the sooner this will appear.



(a) Fourier spectrum on the white lines shown in Fig. 3(b)



(b) The effect of changing the spatial resolution

Figure 3: Time evolution of solution of the HKdV equation with $P = 4\pi$, $\alpha_1 = 1.0$, $\alpha_2 = 0.05$, $\beta = 111.11$, $A = 2.0$

5.2 Upper limit on the number of space grid points

There is also an upper limit on the spatial grid resolution. Unlike the FD methods where the computational cost is the limiting factor, the PS methods have a different kind of a problem, related to computer's numerical precision.

All of the numerical calculations in this study have been done with 64-bit or *double precision* numbers. These numbers can represent a signed decimal number with 16 significant places and exponent range of ± 308 . Subtraction and addition operations will increase this numerical error, so the results from most of the FFT software have a precision of about 13 or 14 decimal places.

The problem is that differentiating in the pseudospectral method can amplify these numerical errors or oscillations. To differentiate the u vector n times, it is necessary to exponentiate the k/l wavenumber vector by n as shown in Eq. (12). Looking at Eq. (11) this means that some elements of the FFT spectrum are multiplied by a magnitude of up to $\left(-\frac{N}{2l}\right)^n$ when taking derivative with

$$\frac{\partial^n u(x, t)}{\partial x^n} = F^{-1} \left[\left(\frac{i \left[-\frac{N}{2}, -\frac{N}{2} + 1, \dots, -1, 0, 1, \dots, \frac{N}{2} - 2, \frac{N}{2} - 1 \right]}{l} \right)^n F u \right] \quad (13)$$

The vector $(k/l)^n$ in Eq. (13) can make the oscillations from FFT become apparent with high derivatives and wavenumbers, so it is extremely important when considering the extent of wavenumber filtering. Between the maximum representable accuracy and the computer's zero lies a region where FFT results oscillate. In the pseudospectral differentiation these oscillations of magnitude $10^{-13} \dots 10^{-14}$ are multiplied with $(k/l)^n$ vector (maximum magnitude element $((-N/2)/l)^n$). The result can easily exceed 10^{14} (depending on n , N and l). This makes the oscillations visible in the $\frac{\partial^n u}{\partial x^n}$ vector.

An example presented in Appendix A explains the issue further, but for this study, the worst case 2π -foldness of the period is $l = 1$, order of differentiation is $n = 5$ and maximum unfiltered $k = 256$ or lower. Thus the maximum magnitude element that the vector $F(u)$ is multiplied with is $(256/1)^5 \sim 10^{12}$, yielding about 4 decimal places of precision before the timestep.

5.3 Filtering

It is evident that, in nonlinear problems, the pseudospectral method requires delicate balance between aliasing errors from too coarse grids and dominating higher derivatives from too fine grids. In case of too fine grid, it is even possible to run out of the computer's numerical resolution. Filtering can then be used to obtain a stable solution, optimise the computational time and allow for greater range of spatial resolution N to be used. In this work, the filter from Salupere's paper [6] is used:

$$f(k, k_1, k_0) = \begin{cases} 1, & -k_1 \leq k \leq k_1, \\ 0, & k \geq k_0, k \leq -k_0, \\ \sin^2 \frac{k+k_0-2k_1}{2(k_0-k_1)}\pi, & k_1 < k < k_0, \\ \sin^2 \frac{k-k_0+2k_1}{2(k_1-k_0)}\pi, & -k_1 > k > -k_0. \end{cases} \quad (14)$$

Here the wave numbers $|k| < k_1$ are passed (multiplied by 1), wave numbers $k_1 < |k| < k_0$ are partly suppressed and wavenumbers $|k| > k_0$ are zeroed. Moreover, the Nyquist wavenumber is zeroed even if no filter is applied. Thus, instead of using wavenumbers (11) in formula for derivatives (12), the filtered wavenumbers $k_f = kf(k, k_1, k_0)$ are to be used. Further considerations for optimal selection of the filtering points k_0 and k_1 is explained by Salupere in [6].

5.4 Shape of the initial profile

The initial profiles considered in Sec. 3 are well-suited for PS methods. The PS method relies on the DFT of the function. When using Fourier transform, the Gibbs phenomenon must be considered. It states that any discontinuities in one domain (original/Fourier) will generate oscillations in the other (Fourier/original) [18]. Oscillations from Gibbs phenomenon are unphysical and unsuitable for simulation at hand. Additionally, the model equation is nonlinear and any oscillations can render the solution unstable and destroy it.

Due to the Jacobi elliptic functions all having derivatives [11],

$$\frac{d(\operatorname{sn} z)}{dz} = \operatorname{cn} z \operatorname{dn} z, \quad \frac{d(\operatorname{cn} z)}{dz} = -\operatorname{sn} z \operatorname{dn} z, \quad \frac{d(\operatorname{dn} z)}{dz} = -m \operatorname{sn} z \operatorname{cn} z,$$

(where m is elliptic parameter) the main initial profile, cnoidal wave (6) also has infinite number of derivatives. This means that the HKdV is to be solved with initial values which are smooth functions and will not generate any oscillations by discontinuities.

5.5 Conserved quantities

According to Eqs. (2) and (3), the HKdV includes two KdV operators. Therefore, knowing that the first two conservation laws of KdV result in periodic conserved densities [5]

$$C_1 = \int_0^P u dx \quad \text{and} \quad C_2 = \int_0^P u^2 dx,$$

then for the HKdV these are

$$C_1 = \int_0^P (u + \beta u_{xx}) dx$$

and

$$C_2 = \int_0^P \left(\frac{u^2}{2} + \beta \left(\frac{u^2}{2} \right)_{xx} \right) dx = \int_0^P \left(\frac{u^2}{2} + \beta [(u_x)^2 + uu_{xx}] \right) dx$$

In the discrete case these will be

$$C_1(t) = \sum_{i=1}^N (u(x_i, t) + \beta [u(x_i, t)]_{xx})$$

and

$$C_2(t) = \sum_{i=1}^N \left(\frac{1}{2} u(x_i, t)^2 + \beta [(u(x_i, t)_x)^2 + u(x_i, t)u(x_i, t)_{xx}] \right).$$

The relative deviations of these conserved densities are verified before analysing the results. It has been found that large relative deviations correlate well with numerical errors visible in wave profile. In case of insufficient accuracy, the profile is to be solved again with refined spatial resolution and with less wavenumbers filtered out.

6 Analysis tools and methods

In this section, various analysis indicators for the wave profiles are explained, illustrated and plotted with an example analysis of the following solution. The IC is in the form of Eq. (6):

Shape	cnoidal
Amplitude A	1.0
Period P	2π
α_1	0.4
α_2	0.028
β	111.11
parameter m	0.5628
IC	$u_0(x) = 1.0 \cdot \text{cn}^2 \left[x \sqrt{\frac{1.0-\eta}{12 \cdot 0.4}}, \sqrt{0.5628} \right], \quad 0 \leq x < 2\pi$

6.1 Direct tools

The direct tools are used to analyse the wave profile without transforming it. Under this subsection are listed various plotting methods used in analysing for solitons.

6.1.1 Pseudocolor plot

Pseudocolor plot is one of the most important tools in analysing the behaviour of the solution as it offers a complete overview at a single glance. It is straightforward to find the number of emerged solitons, the existence of tail and the points of interactions between the solitons.

Since the main interest of this work lies in the small and hidden solitons, a nonlinear, exponential colormap is used. Let the normalised range $u \in (0, 1)$ be the range to be mapped, then the color is mapped in range u^a where a is the colormap nonlinearity parameter, to be specified by the user when analysing the plot. Parameter $a = 1$ would yield a linear colormap, but for this work, $a = 0.5$ has been found to give good results and allows the small differences at low amplitudes to be seen more clearly.

The pseudocolor plot (over two space periods, as most of the pseudocolor plots in this work) of the example is shown in Fig. 4 along with its colormap. The interaction times coincide with time points t_k , as in Salupere [6] and also explained in the upcoming subsection 6.3. A train of 3 solitons is clearly visible with recurrence at time t_1 . At moment t_2 the first soliton interacts with third. Also shown is the time moment t_3 , which is explained further along.

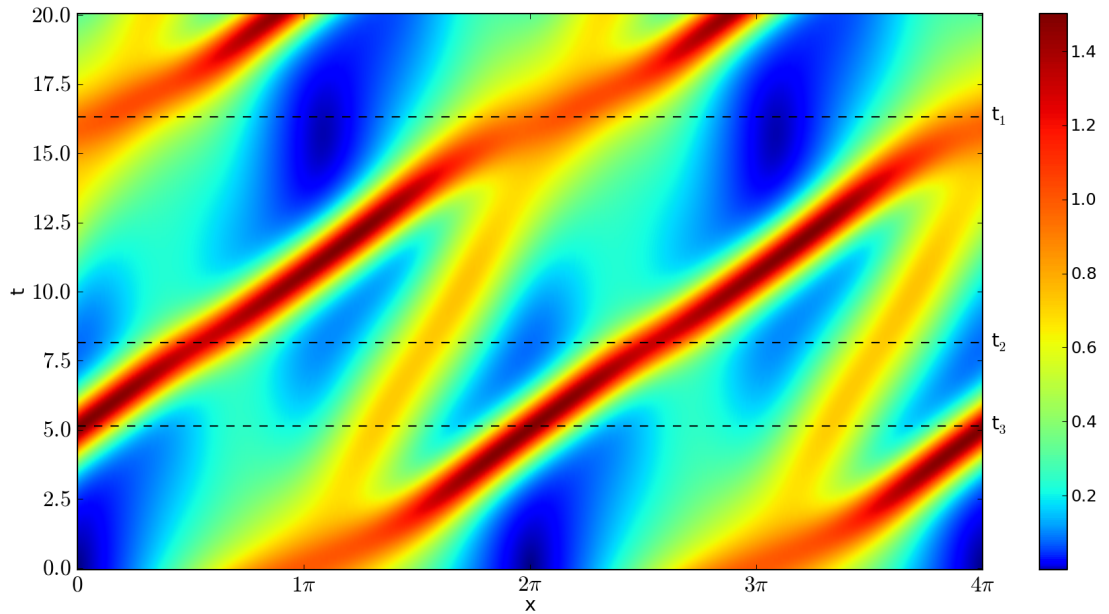


Figure 4: Pseudocolor plot of the example case (two space periods)

6.1.2 Wave profile maxima curves

The maxima curves trace the evolution of maxima of the solution and show the change of amplitudes of various humps of the solution. As solitons are by definition extremely stable waves, any changes of the solution maxima must correspond to either evolution of the initial wave into separate solitons or, alternatively, the interaction between various solitons (of different amplitudes). While the hidden solitons are often too small to be detected *directly* from the solution by peak-detection algorithms, they do visibly affect larger soliton amplitudes by interaction. This makes amplitude curves one of the most important tools in analysing the soliton formation and interactions.

The maxima curves for the current example are shown in Fig. 5. The same interactions that were seen in pseudocolor plot can be seen here too. There is an additional,

unnaturally flat region in the maxima curve of the highest soliton centered on time t_3 . This means that there is a fourth, hidden soliton in the wave profile interacting with the highest soliton at that time. Its influence on the second soliton can be seen at t_2 . This fourth soliton could not be directly detected from the pseudocolor plot in Fig. 4.

The fourth soliton is barely detectable, even on the maxima curves it manifests only as a flat region. When the hidden soliton cannot be detected because it is coincident with a larger soliton, another time of interaction (with less background fluctuation) might be observed instead: for the solution at hand it happens on time $t \approx 11$. On maxima curves in Fig. 5 this manifests as another concave region in the largest maxima curve and on pseudocolor plot in Fig. 4. A straight line could be drawn from the point where solitons emerge and through these two points where the first and the fourth solitons interact. This is expected and corresponds with the definition of hidden soliton [3].

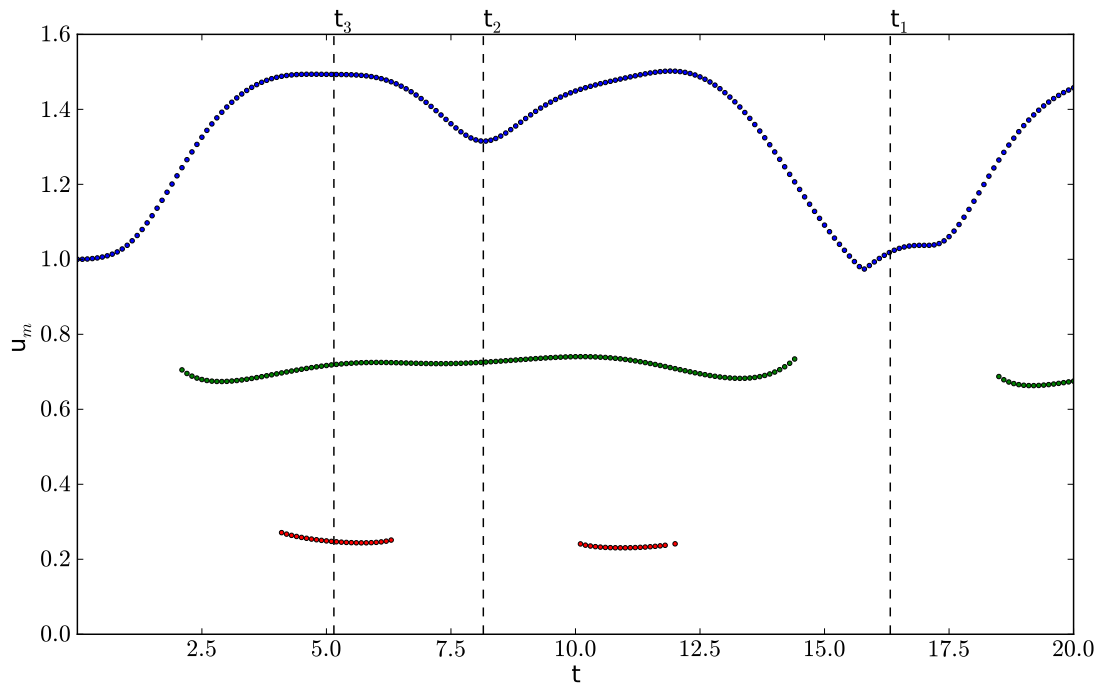


Figure 5: Maxima curves of the example case

As the maxima of various peaks in some given time t are taken on discrete values of $u(x_i, t)$, the maxima curves can appear somewhat distorted, jagged or oscillatory moving through time if the peak is sharp. To that end, the peak-finding algorithms used in this work are augmented with code that corrects these problems and finds the true maxima between the spatial grid points by using the Fourier transform and its

shifting theorem. The true maxima is found by Newton iteration scheme

$$x_{n+1} = x_n - \frac{f'}{f''}, \quad \text{where} \quad f' \rightarrow 0,$$

near the approximate (on-grid) maxima points. This iteration of shift theorem is continued until $|f'(x)| < \varepsilon$ (ε being the error tolerance). Since this is a computationally intensive task, it was written in Fortran and wrapped to Python with f2py [17].

6.2 Discrete Spectral Analysis

In the same sense that the pseudospectral method is global, the DSA characterises the wave profile globally, based on its Fourier spectrum. The analysis tools described in this subsection are taken from Salupere's paper [6] and are here only briefly referred.

6.2.1 Spectral amplitudes and spectral densities

The DFT spectrum $U(k, t)$ of an arbitrary wave profile $u(x, t)$ is generally complex, so it can be characterised by magnitude $|U(k, t)|$ and argument $\phi_k(t)$. Defining the multipliers

$$\begin{aligned} a_0(t) &= \frac{U(0, t)}{N}, \\ a_k(t) &= \frac{2|U(k, t)|}{N}, \quad k = 1, 2, \dots, \frac{N}{2} - 1, \\ a_k(t) &= \frac{|U(k, t)|}{N}, \quad k = \frac{N}{2}, \end{aligned}$$

it is possible to synthesise the waveform using cosine series

$$u(x, t) = a_0(t) + \sum_{k=1}^{N/2} a_k(t) \cos[kx + \phi_k(t)].$$

Here the quantities $a_k(t)$ are called *spectral amplitudes* and $\phi_k(t)$ is the *phase spectrum*.

Parseval's theorem is widely known to describe the energy spectrum of the system, in this case at a fixed time t .

$$\sum_{j=0}^{N-1} [u(x_j, t)]^2 = \frac{1}{N} \sum_k |U(k, t)|^2$$

The distribution of this energy between different modes can thus be characterised by *spectral densities* [6]

$$S(k, t) = \begin{cases} \frac{2|U(k, t)|^2}{N} = \frac{Na_k^2}{2}, & k = 1, 2, \dots, \frac{N}{2} - 1 \\ \frac{|U(k, t)|^2}{N} = Na_k^2, & k = \frac{N}{2} \end{cases} \quad (15)$$

and the Parseval's theorem written [6]

$$\sum_{j=0}^{N-1} [u(x_j, t)]^2 = \frac{[U(0, t)]^2}{N} + \sum_{k=1}^{N/2} S(k, t). \quad (16)$$

In the results of this work, the spectral amplitudes and their peaks will be used for analysis. The spectral amplitudes of the example are shown in Fig. 6.

6.2.2 Cumulative spectrum and time averaged normalised spectral densities

The spectral densities can be normalised by total energy. When summed cumulatively starting from higher wavenumber modes it yields *cumulative spectrum*. It reflects the summed energy of those harmonics. Among other purposes it can be used to estimate the amount of wavenumbers needed to be left unfiltered. Alternatively, the normalised spectral densities could be integrated over time, resulting in the *time averaged normalised spectral densities*. This shows the contribution of a spectral density over the analysis time interval. These measures are discussed in detail in [6].

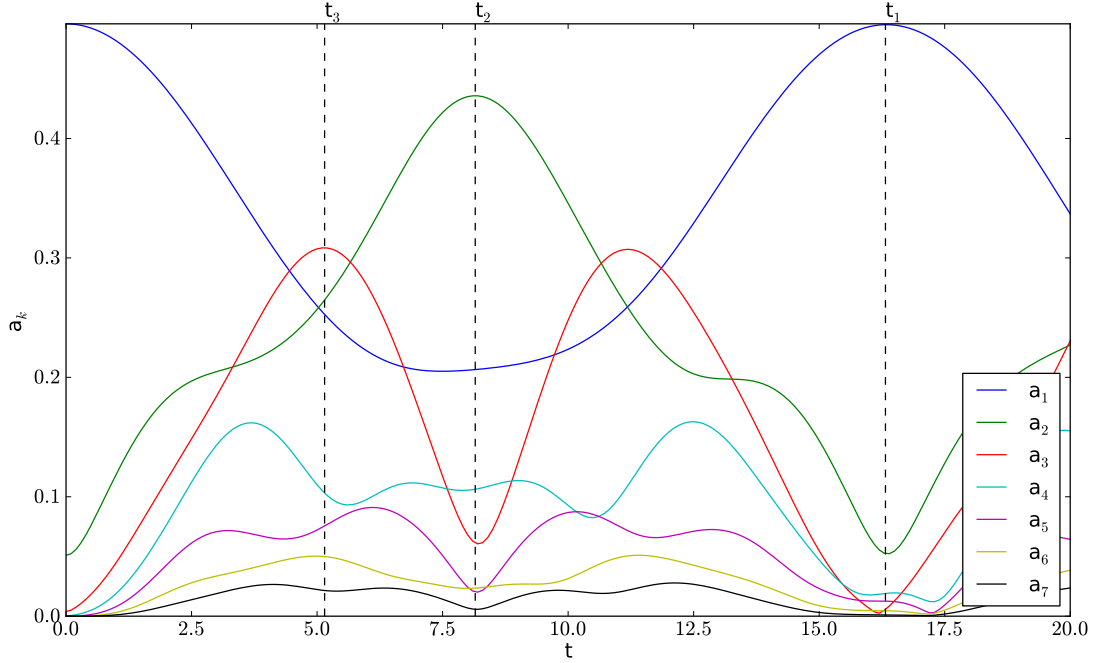


Figure 6: Spectral amplitudes of the example case

6.3 Spectral detection of hidden solitons

Salupere [6] shows how to find the total number of solitons (including the hidden ones) in case of KdV equation with harmonic IC using the spectral amplitudes or spectral densities and maxima curves. Using the spectral amplitude curves, the time moments t_k are introduced, where t_1 stands for the time of the first recurrence (“when the initial spectral state is almost restored”) and the time moments t_k ($k > 1$) “correspond to the maximum value of the k -th spectral amplitude a_k in the time interval $0 < t < t_{k-1}$ ”. As a rule these maxima are global in $0 < t < t_1$. In that case:

- Every interaction between solitons is reflected by a local minimum or concavity in the higher soliton’s amplitude curve.
- If the time of the first maximum of the k -th spectral curve is denoted as t_k , then:
 - The first and k -th soliton interact for the first time near the time moment t_{k-1} .
 - The second and k -th soliton interact for the first time near the time moment t_{k-2} and so on.

To determine the number of hidden solitons, it is important to know the number of visible ones. Salupere [2] defined that hidden solitons are those which remain hidden in the *initial* soliton train. This means that the solitons which emerge until the first interactions (time moment where the largest soliton's maximum curve starts decreasing) are visible solitons. A train of visible solitons for the example solution is shown in Fig. 7.

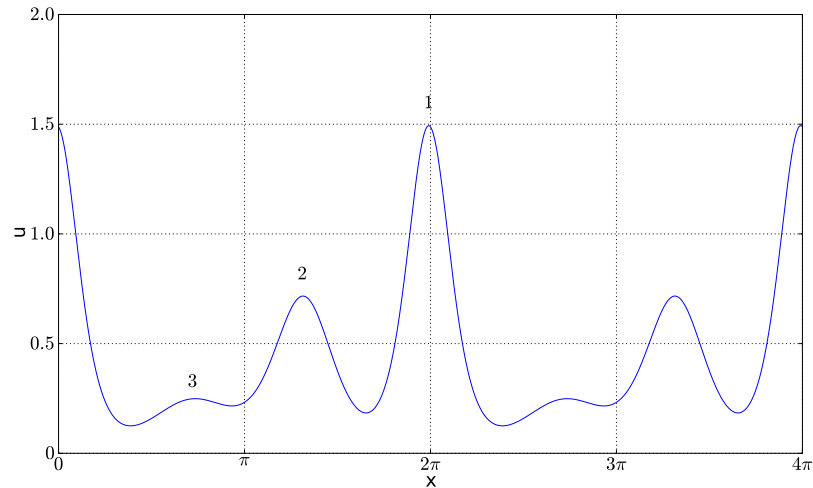


Figure 7: Slice over two periods of the example solution at time $t = 5.0$ showing 3 visible solitons

Salupere [6] shows how the total number of solitons can be found by locating the earliest indication of a small soliton from the maxima curves and then identifying the solitons interacting at that point. The interaction points are recognized by a local minimum or concavity in the higher soliton's maximum curve. The smaller soliton is then identified from maxima curves, pseudocolor plot or spectral amplitudes.

The recurrence, mentioned earlier, means the reconstruction of the initial state through nonlinear interactions [13]. It is best ascertained from the spectral amplitudes [6].

For this work, the tools for Discrete Spectral Analysis were developed with the packages SciPy [19] for backend, f2py [17] for making Fortran routines available in Python and Enthought Tool Suite for visualisation [20].

6.4 Parameter space

The initial value problem for the HKdV equation (1) includes several parameters which can be varied in numerical experiments and analysis. At first, three parameters in the HKdV equation: dispersion parameters α_1 and α_2 , and the microstructure parameter β . Secondly, parameters that are involved in initial conditions: amplitude A , spatial period P and the ICs also depend on the dispersion parameter α_1 via the requirement that the macrostructure KdV operator satisfies $\psi_1 = 0$. The cnoidal initial wave (6) has the parameter m which in this work is acquired from Eq. (5) from amplitude A , period P and dispersion parameter α_1 .

Ilison [5] analysed the parameter space of HKdV with 16π long sech^2 initial profile suiting the first KdV operator in HKdV and demonstrated the following properties:

- For $\beta \leq 0.1111$, the number of emerging solitons is always one when $\alpha_1 > \alpha_2$.
- If $\beta \geq 1.111$ and again $\alpha_1 > \alpha_2$, the number of solitons increases with the ratio α_1/α_2 increasing.
- Generally, a tail of oscillations will also be generated besides the solitons.
- In cases where $\alpha_1 < \alpha_2$, the wave profile will consist mostly of one hump and the tail. In the limiting case where α_1 is much smaller than α_2 , the hump will disappear in the forming wave packet.
- HKdV where $\alpha_1 = \alpha_2$ leads to ordinary KdV and can be used for checking purposes but is not interesting.

In this thesis, it was found that there exist ratios between α_1 and α_2 where the solution is relatively free of the tail and “clean”. These ratios form probably because of some agreement between micro- and macrostructure at the specific parameter values, as shown in Fig. 8. For the problem at hand, the “clean” or tailless solutions are of interest because they allow to detect the small, hidden solitons without the oscillations of the tail getting in the way. Consequently, the solutions analysed in this work have parameters α_1 and α_2 selected so they would minimize the oscillatory tail.

These “clean” ratios were discovered at $\beta = 111.11$ but when scanning the same region of $\alpha_1 - \alpha_2$ space with $\beta = 11.111$, these ratios were much less pronounced and

harder to detect from the array of solutions with tails. It is as if the bands of α_1/α_2 , where “clean” solutions emerge are smeared and the energy “leaks out” of the solitons as they propagate through time. Moreover, the solutions seem to retain some background fluctuation (Fig. 9(b)) in $\beta = 11.111$ case, when compared to solution with $\beta = 111.11$ (Fig. 9(a)). These effects decrease with α_1 and α_2 decreasing. With small dispersion parameters, the solution of $\beta = 11.111$ will resemble the case $\beta = 111.11$ better, including the ratios of α_1/α_2 which produce solutions with smallest tail. In the following study β is taken $\beta = 111.11$ to facilitate “cleaner” solutions with less oscillations disturbing the analysis and finding of hidden solitons.

Ilison [5] uses sech^2 -shaped IC and thus notes that the change of amplitude does not change the essence of the solutions, but merely the speed of the propagation and in some cases the shape of the trajectory. However, as in this work the cn^2 -shaped IC is used then the shape (given by elliptic parameter m) depends on the amplitude. Thus here the change of amplitude *does* change the type of the solution, number of emerging solitons, the existence of tail and the emergence of the hidden solitons.

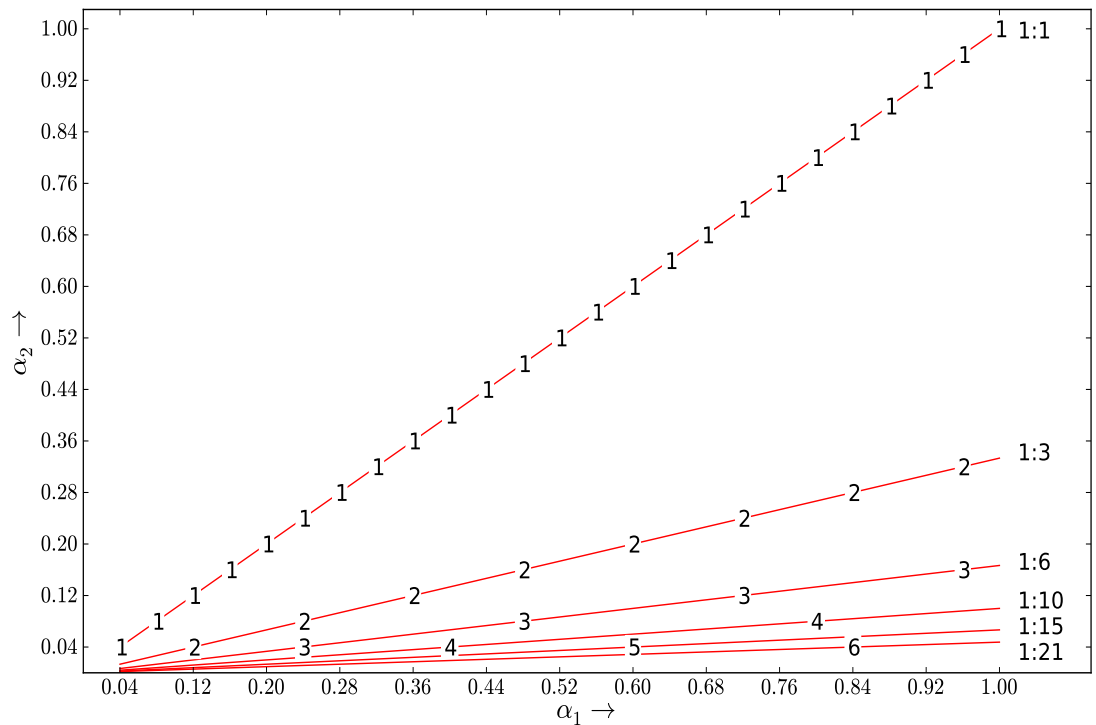
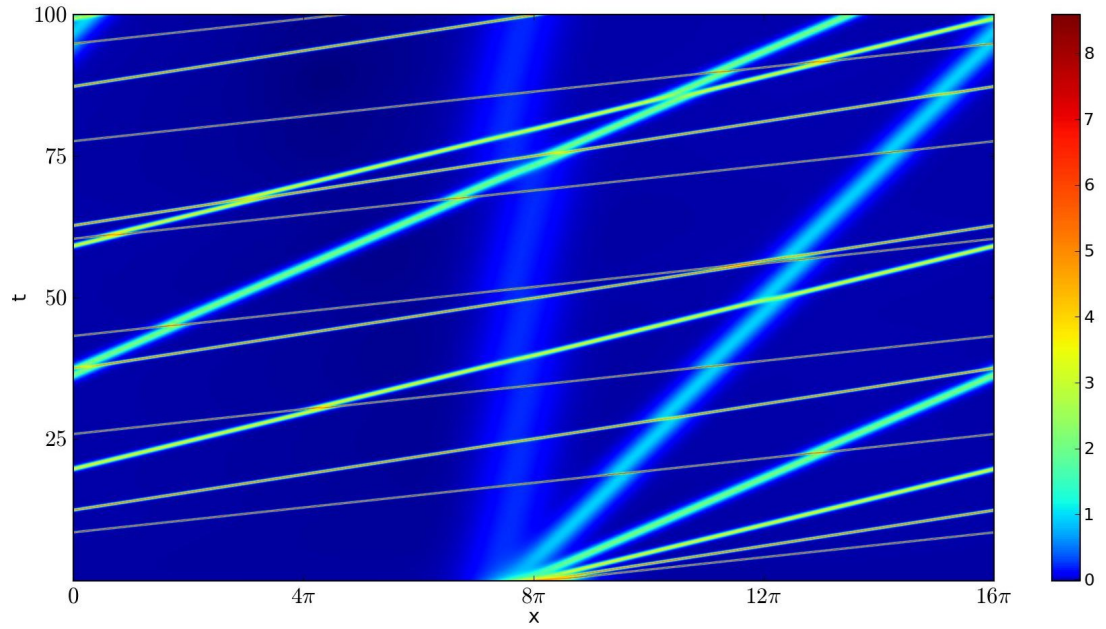
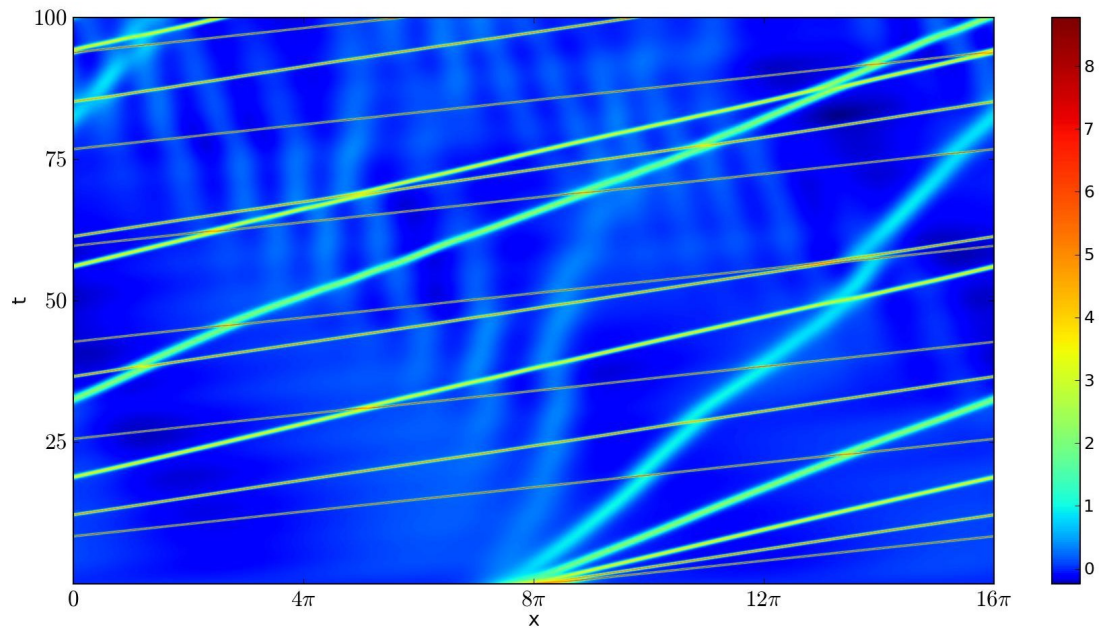


Figure 8: Number of emerging solitons against parameters α_1 and α_2 ($N = 1024$, $P = 16\pi$, $\beta = 111.11$, amplitude = 5.0, sech^2 initial profile)



(a) Pseudocolor plot ($\beta = 111.11$)



(b) Pseudocolor plot ($\beta = 11.111$)

Figure 9: The effect of changing the β (single period, $N = 4096$, $P = 16\pi$, amplitude = 5.0, sech^2 initial profile $\alpha_1 = 0.84$, $\alpha_2 = 0.04$)

7 Results and discussion

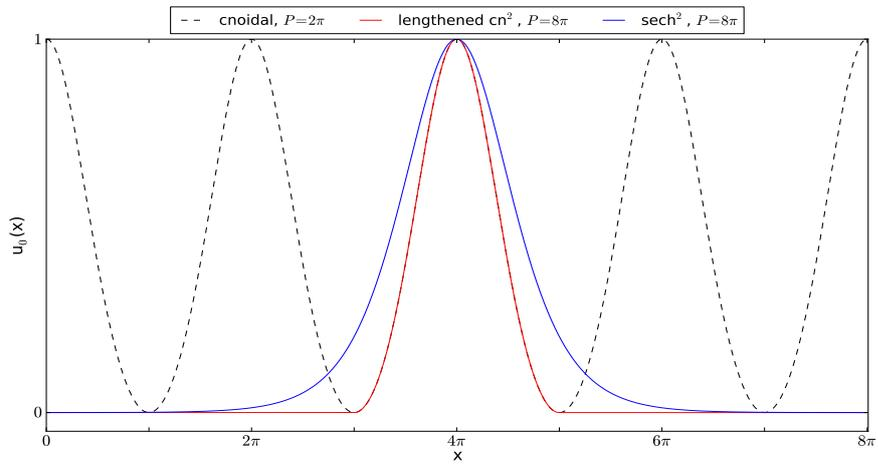
In this section, the solutions of the HKdV are presented and analysed using the tools introduced in Sec. 6. Firstly is studied the influence of the elliptic parameter m ; secondly the influence of microstructural dispersion parameter α_2 ; and thirdly the influence of amplitude A and macrostructural dispersion parameter α_1 .

7.1 The influence of the initial wave on the results

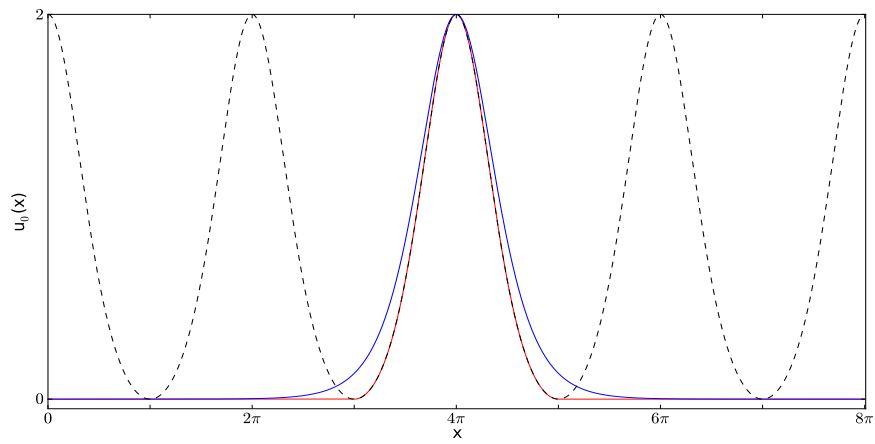
The impact of the shape of the initial cnoidal wave on the resulting solution is subsequently analysed. In this work, the elliptic parameter m (see Sec. 3.1) of the cnoidal initial waves ranges from $m = 0.5628$ (closer to harmonic wave, shown by dashed line in Fig. 10(a)) to $m = 0.9905$ (closer to sech^2 -shaped wave, shown by dashed line in Fig. 10(c)). The parameter m is changed indirectly by varying the initial amplitude A and the macrostructural dispersion parameter α_1 .

The base results are from cnoidal initial wave ($P = 2\pi$). They are compared with the results from sech^2 -shaped ICs ($P = 8\pi$, $m = 1$) and with lengthened cn^2 -shaped ICs ($P = 8\pi$, parameter m is not applicable). Therefore the parameter m in Table 1 is applicable *only* to the results from cnoidal initial waves. The hidden solitons arise most naturally from the cnoidal $P = 2\pi$ wave. Conversely, $P = 8\pi$ results from sech^2 and lengthened cn^2 shaped initial waves leave more room for the wave train to expand before and between the interactions. The range of used initial wave shapes is displayed in Fig. 10.

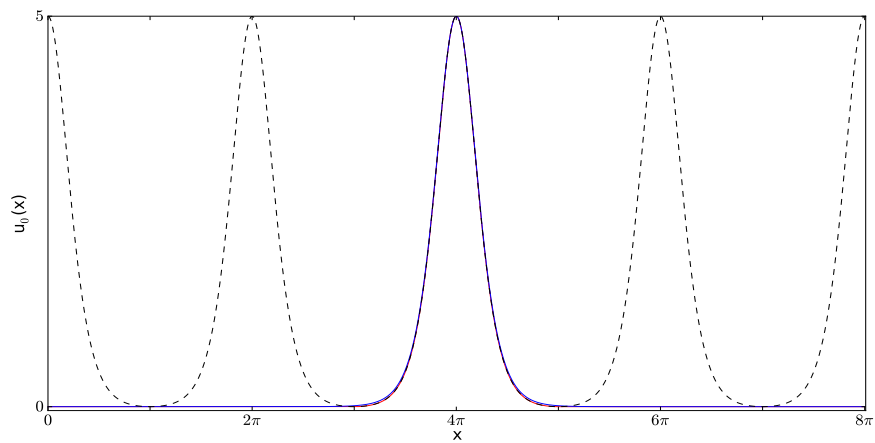
Table 1 summarises the number of visible solitons in columns “No. sol.-s” where the number of hidden solitons are shown in parentheses. The concurrency of the interactions with spectral amplitudes is shown in columns “SA fit” (see Sec. 6.3) ranging from low m to high m shapes of the IC. The existence of tail in the solution is indicated by “t.”, strong tail by “s.t.” and weak tail by “w.t.”.



(a) ICs for $m = 0.5628$



(b) ICs for $m = 0.8027$



(c) ICs for $m = 0.9905$

Figure 10: Initial conditions

Table 1: Character of the solution against parameters m , A , α_1 and α_2 . Solutions are calculated up to the interaction between the two highest solitons.

m	A	α_1	α_2	cn ² & 2 π		cn ² & 8 π		sech ² & 8 π	
				No. sol.-s	SA fit	No. sol.-s	SA fit	No. sol.-s	SA fit
0.5628	1.0	0.4	0.0055	6(+1)	All	7+t.	a_4	9(+2)	a_4
			0.0280	3(+1)	All	3+t.	a_2	5	a_2
0.3		0.0255	3(+1)	All	3+t.	a_2	4	a_2	
		0.0420	2(+1)	All	2+s.t.	a_1	3	a_2	
0.6663	2.0	0.4	0.0055	7(+2)	a_1-a_5	9+t.	a_4	10(+1)+w.t.	a_4
			0.0280	4	All	4+t.	a_2	5	a_2
0.8027	3.0	0.3	0.0255	3(+1)	a_1-a_2	4+t.	a_2	4	a_2
			0.0420	3	All	3+t.	a_2	3+w.t.	a_2
0.8807		0.4	0.0055	8(+2)	a_4, a_5	10+t.	a_4	10(+1)+w.t.	a_4
			0.0280	4(+1)	a_2	4+t.	a_2	5	a_2
0.9063	4.0	0.3	0.0255	4	a_2	4+t.	a_2	4+w.t.	a_2
			0.0420	3(+1)	a_2	3+t.	a_2	3+t.	a_2
0.9530		0.4	0.0055	8(+2)	a_4	10+t.	a_4	10(+1)+w.t.	a_4
			0.0280	4(+1)	a_2	5+t.	a_2	5	a_2
0.9530	5.0	0.3	0.0255	4	a_2	4+t.	a_2	4+t.	a_2
			0.0420	3(+1)	a_2	3+t.	a_2	3+t.	a_2
0.9797		0.4	0.0055	8(+3)	a_4	11+w.t.	a_4	11+w.t.	a_4
			0.0280	4(+1)	a_2	5+w.t.	a_2	5	a_2
0.9751	5.0	0.3	0.0255	4(+1)	a_2	5+t.	a_2	4+t.	a_2
			0.0420	3(+1)	a_2	4+t.	a_2	3+t.	a_2
0.9905		0.4	0.0055	8(+3)	a_4	11+w.t.	a_4	11+w.t.	a_4
			0.0280	4(+1)	a_2	5+w.t.	a_2	5	a_2
0.9905	0.3	0.0255	4(+1)	a_2	5+t.	a_2	4+t.	a_2	
		0.0420	3(+1)	a_2	4+t.	a_2	3+t.	a_2	

7.1.1 The emergence of hidden solitons and tail

Firstly, looking at Table 1, it can be seen that the parameters have been chosen successfully: many solutions include hidden solitons while most of them are tailless or exhibit only a small tail. The distinction between the hidden soliton and the tail can nevertheless be difficult. In this thesis it is based on the properties of a soliton: it must have a

bell-like shape, be stable, have elastic interactions and constant speed. Conversely, the tail oscillates about a certain reference level (Fig. 11).

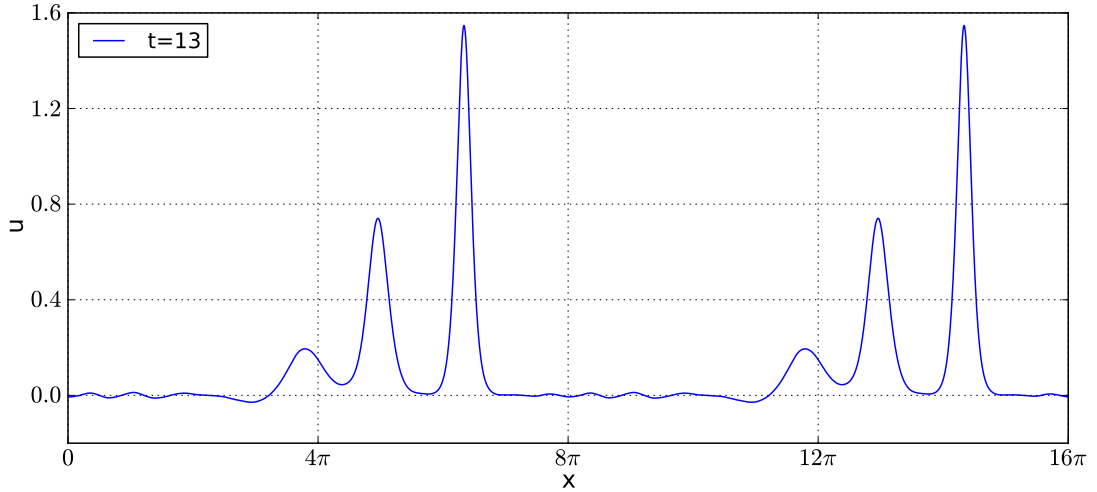


Figure 11: Three solitons and a tail (lengthened cn^2 IC where $P = 8\pi$, $A = 1$, $\alpha_1 = 0.4$, $\alpha_2 = 0.028$, two spatial periods)

As hoped, the cnoidal initial wave with its short, $P = 2\pi$ period allows to generate solutions where the emerging solitons start interacting before the train is fully formed, generating hidden solitons. Furthermore, the corresponding lengthened cn^2 -shape IC generates comparable number of solitons which are all usually visible. Unfortunately, the number of solitons is not always identical: for half of the solutions, lengthened cn^2 IC generates one soliton less than the cnoidal wave. This discrepancy decreases as amplitude A increases (Table 1).

At high amplitudes A , all initial waves coincide better (Fig. 10(c)). This means that the sech^2 -shaped IC closely matches the lengthened cn^2 wave. This in turn means that now the sech^2 -shaped IC can also predict the number of solitons emerging from the cnoidal initial wave. Furthermore, the sech^2 IC and its results coincide with ones from cnoidal wave when the parameter $m \rightarrow 1$. This shows that when the parameter m of the cnoidal wave $m \rightarrow 1$, the period length is not too important in determining the total number of emerging solitons (Fig. 10(c)) (nevertheless m still depends on it). The sech^2 -shaped ICs and solutions are generally distinct from cn^2 -shaped ICs and their solutions. With a broader pulse (Fig. 10(a)) the sech^2 -shaped initial wave can also generate hidden solitons when the emerging soliton train is sufficiently long.

Generally the number of hidden solitons mostly depends on the period length and the total number of emerging solitons. These control whether the soliton train can fully emerge before the interactions begin. These hidden solitons affect the visible ones via the interactions.

The tail cannot be detected in results from cnoidal $P = 2\pi$ waves. Conversely, all $P = 8\pi$ lengthened cn^2 IC results exhibit a tail. It grows weaker as amplitude A increases and shape of this IC approaches that of a $P = 8\pi$ sech^2 -shape. Mostly the results from sech^2 -shaped ICs are tailless, thanks to its smoothness and the fact that it was used in choosing the optimal α_1 and α_2 . When the tail exists in sech^2 IC results, however, the increase in the amplitude also increases the tail. This is the opposite from the lengthened cn^2 IC.

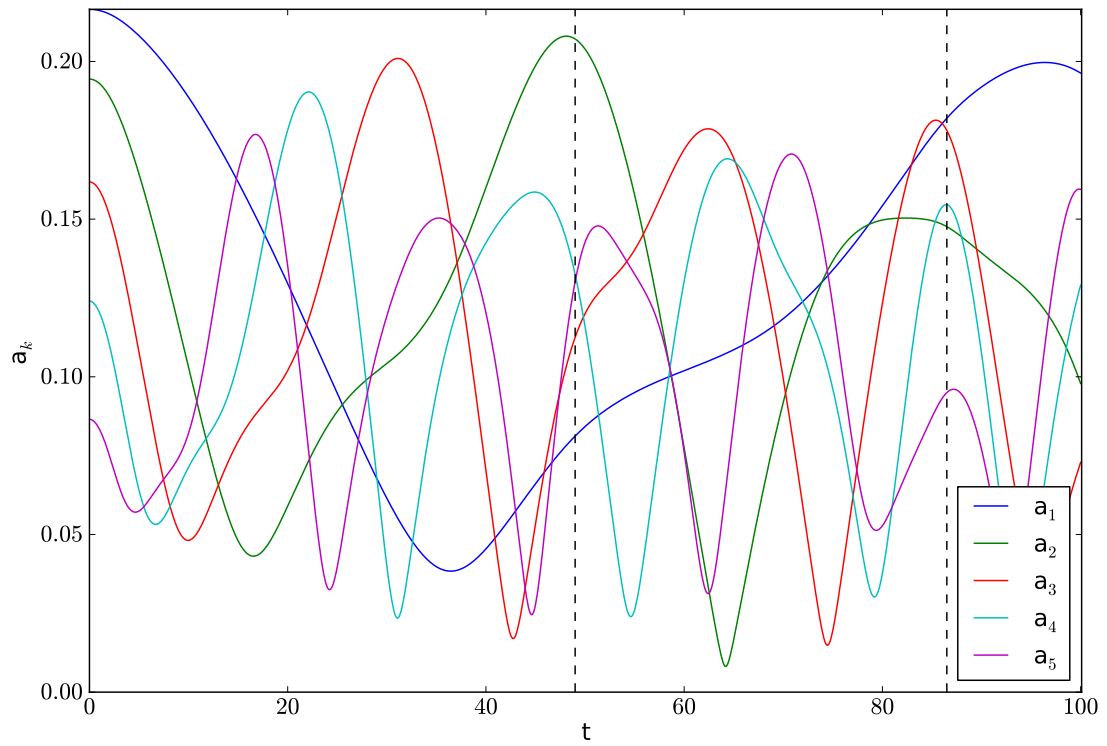
As the model equation and initial waves analysed here are quite general, the interaction concavities remain the most important method for detecting the hidden solitons. The maxima curves exhibit a concavity or a local minimum where the soliton interacts with a smaller one. In conjunction with pseudocolor plot, enough such evidence can usually be found to detect the hidden solitons.

Based on these results, the spectral analysis methods are further examined.

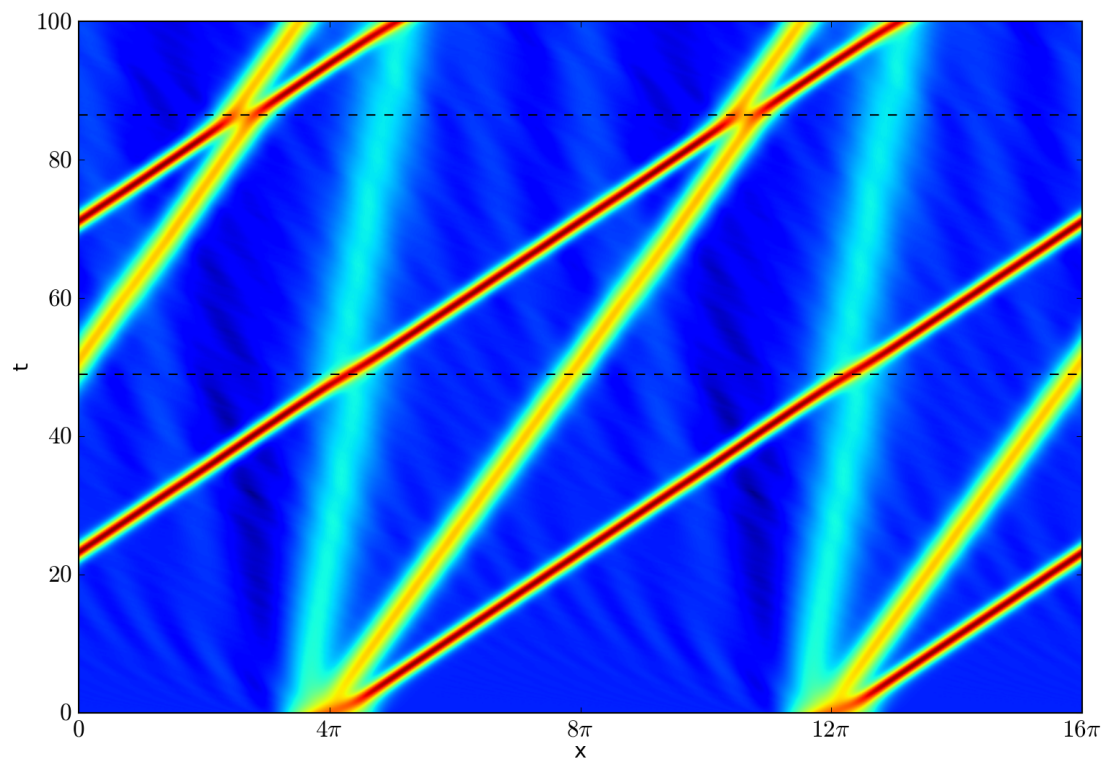
7.1.2 The concurrency of the interactions with the spectral amplitude peaks

Figure 12(b) displays how in a typical lengthened cn^2 IC solution, the third soliton misses the first interaction of the two largest solitons. In the example case (Fig. 4) all solitons interacted at the same point. This recurrence of the initial state is best seen spectrally: the first peak of a_1 is a recurrence for the example case (Fig. 6) but not for the result at hand (Fig. 12(a)). Therefore, for this part of the analysis, the notation t_k is not used because the peaks are not counted backward from the *recurrence*, but from the interaction between the two largest solitons.

Interactions between the first (highest) and the rest of the solitons, up to the interaction of the first and the second, were found. They were compared to the peaks of the spectral amplitudes: any amplitudes a_k , where the peak coincides with the interactions as described in Sec. 6.3 is marked in the Table 1 column “SA fit”.



(a) Spectral amplitudes



(b) Pseudocolor plot

Figure 12: Interaction points shown by dashed lines. Lengthened cn^2 IC where $P = 8\pi$, $A = 1$, $\alpha_1 = 0.4$, $\alpha_2 = 0.028$

It can be seen from Table 1, that for HKdV with cnoidal IC, the interactions between the solitons correspond to the spectral amplitude peaks only for the two lowest values of the parameter m ($m = 0.5628$ and $m = 0.6663$), see the example case Figs. 4 and 6. As the parameter m is increased, usually a single peak of a_k remains coincident with its interaction (for example, the interaction between the first and the third soliton at $t = 47$ and the peak of a_2 in Fig. 12). This single peak depends on the number of emerging solitons. The peaks of other a_k , where k is smaller than this peak, gets delayed with respect to the interaction (a_1 in Fig. 12) and where k is larger than this peak is advanced with respect to the interaction.

The fit between the peak of a_k and interactions depends on the number of emerging solitons. As the number of emerging solitons increases, this spectral prediction of the smallest-largest soliton interactions worsens. For example, the same number of a_k peaks correspond to their respective interactions for cases of $A = 2.0$, $\alpha_1 = 0.3$, $\alpha_2 = 0.0255$ and $\alpha_2 = 0.042$ (Table 1). Since $\alpha_2 = 0.0255$ has an additional fourth, hidden soliton, the peak of a_3 does not correspond to its interaction with the first soliton. As $\alpha_2 = 0.042$ results has only three solitons, it has no such problem.

Increasing the parameter m brings the recurrence to a closer point in time and at the same time makes it worse. The quality of the recurrence regresses as the shape of the cnoidal IC $m \rightarrow 1$ (Fig. 13 where increasing A increases the m) and its time moment advances. As the first peak of a_1 stops being a recurrence, a new recurrence can be found from a peak in the later time (Fig. 13). Obviously, the rest of the emerged solitons no longer interact where the two highest solitons interact for the first time (Fig. 12(b)). This also applies for the $P = 8\pi$ lengthened cn^2 and sech^2 shaped results where the recurrence is generally not on the first peak of the a_1 and happens later due to the periodic space.

To conclude, as the cnoidal initial wave changes from harmonic to non-harmonic, the first recurrence breaks down and the analysis via the spectral amplitudes cannot be used to detect the interactions like it is possible for nearly harmonic ICs.

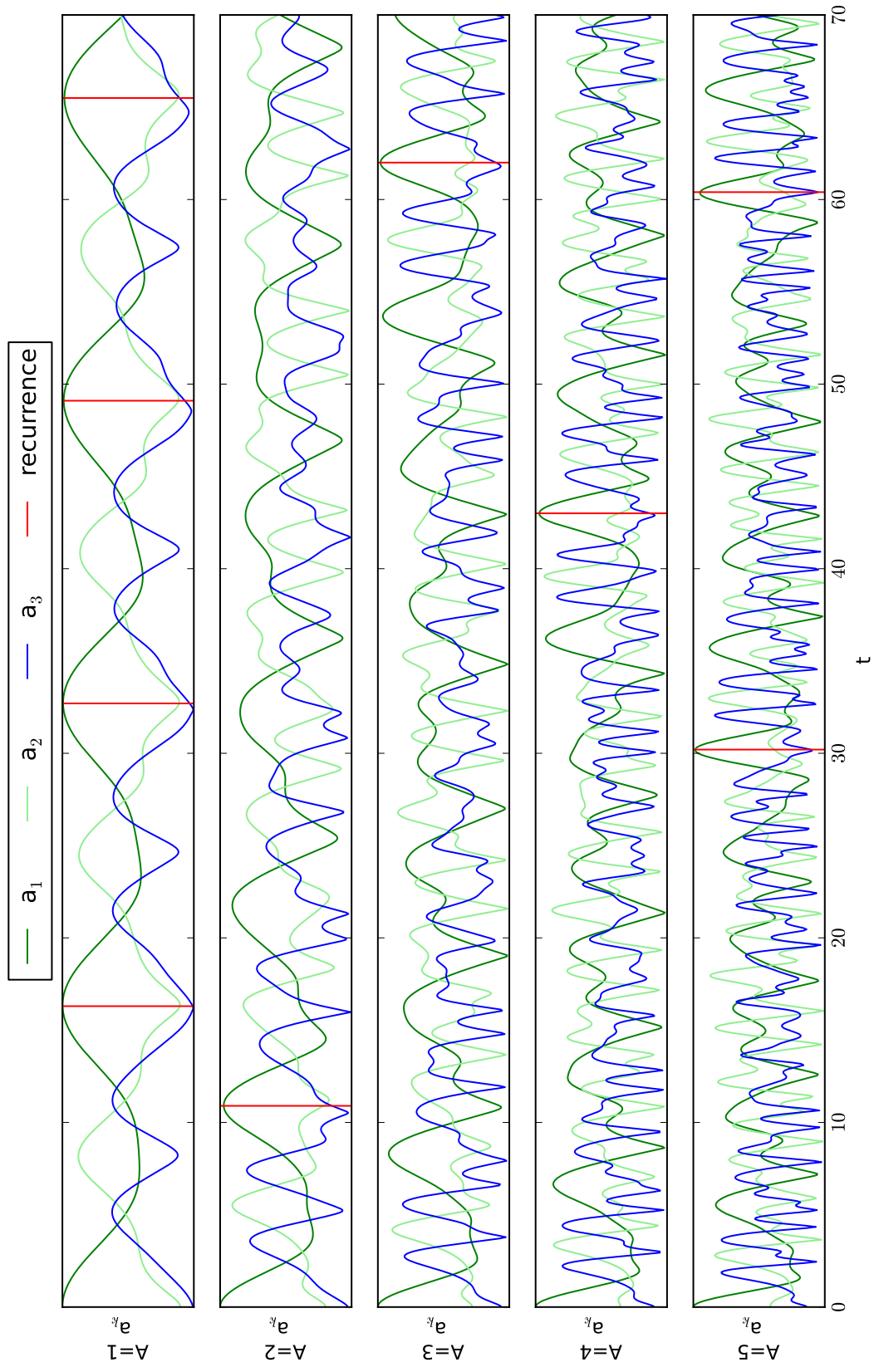


Figure 13: Spectral evolution of solutions of different A (cn² IC, $P = 2\pi$, $\alpha_1 = 0.4$, $\alpha_2 = 0.028$)

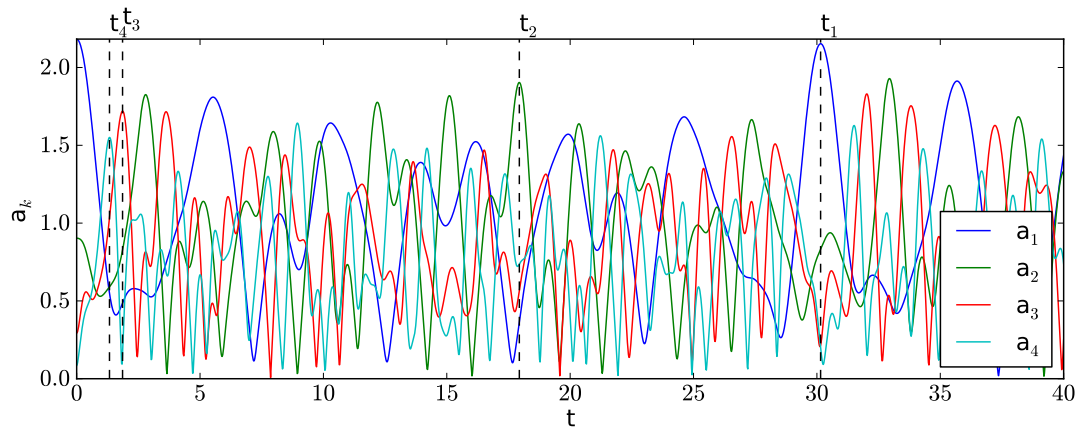
7.1.3 The concurrency of t_k moments with the interactions

As the t_1 should be placed on the recurrence [6], the opposite process to the previous subsection is carried out here. A suitable recurrence is found and other t_k points are located as per Sec. 6.3 and compared to the interactions. Unlike the harmonic ICs where recurrence can be expected at the first a_1 peak, here the solution is generated until a suitable recurrence occurs which, for the cnoidal ICs with high parameter m , can occur on some other peak of a_1 , in a much later time.

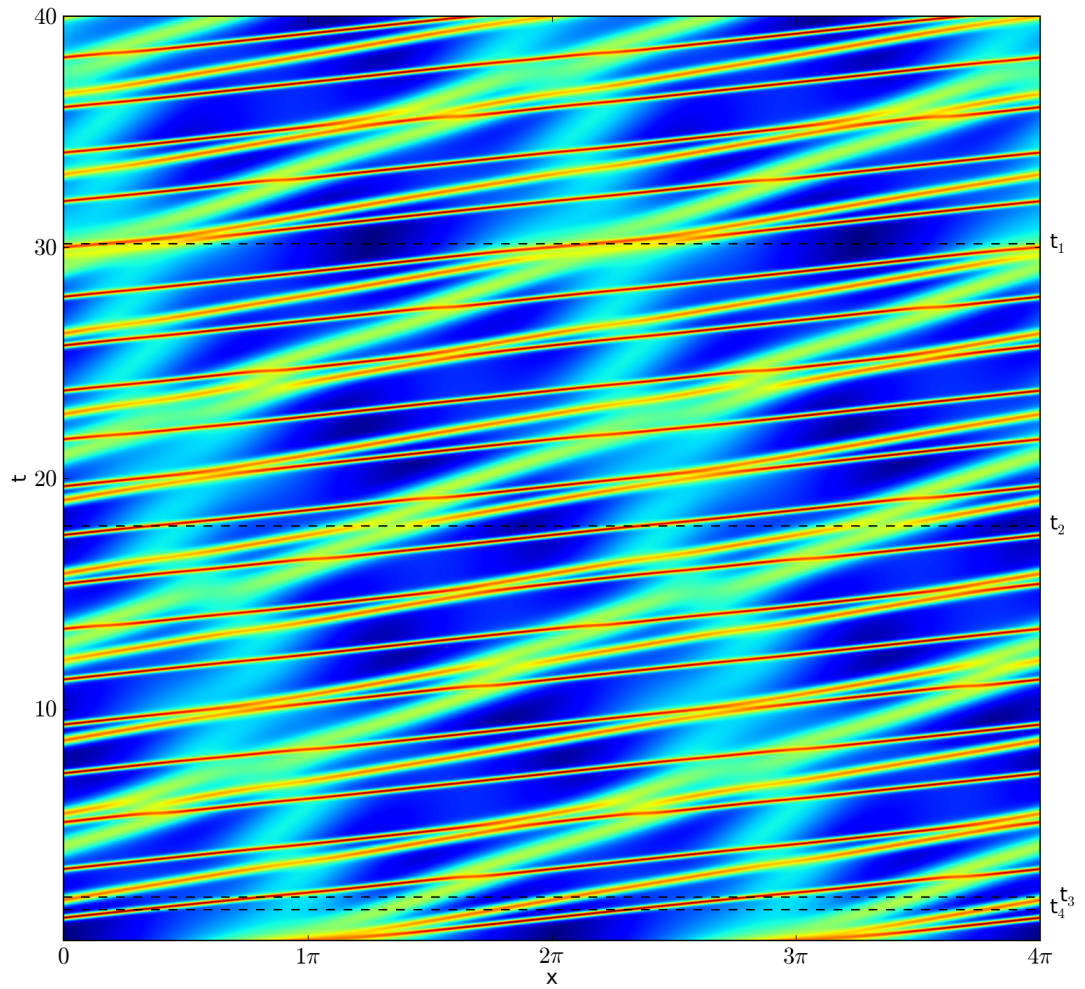
It turns out that the t_k points can be found according to the rules presented in Sec. 6.3 even when the IC-s are not harmonic. Furthermore, these t_k moments reflect some of the interactions. Unfortunately it is difficult to predict which of the interactions happen at the t_k peaks because the total number of interactions before the recurrence can be very high. As soon as the shape of the IC deviates from the harmonic and the first peak of a_1 stops being a good recurrence, the nature of the interactions at t_k start being more unpredictable. For example, in case of the results from lengthened cn^2 or sech^2 $P = 8\pi$ ICs, usually several peaks of a_2 exist with comparable amplitudes that could be t_2 time moments. On those moments, however, various soliton interactions can take place, for example:

- odd and even solitons,
- 1-4 and 2-3 (Fig. 14),
- 1-2 with 3rd soliton at $P/2$ distance (Fig. 15).

In conclusion, as the IC turns nonharmonic, the emerging solitons start missing each other, so it can take much time and many interactions before the recurrence happens. From the large number of available interactions between various solitons, only those that are somehow ordered in the momentary wave profile are reflected by spectral peaks t_k . This means specific solitons interacting at a specific spatial distances, like the $P/2$ distance between the interaction between the first and the second soliton and the location of the third soliton. If the third soliton is at some other distance from the interaction, then the spectral amplitudes are completely different (Figs. 15(a) and 16).

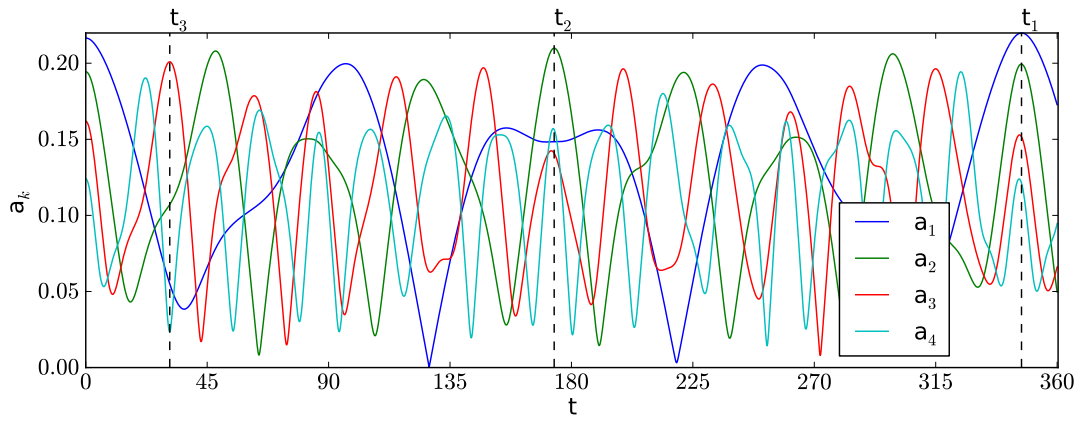


(a) Spectral amplitudes

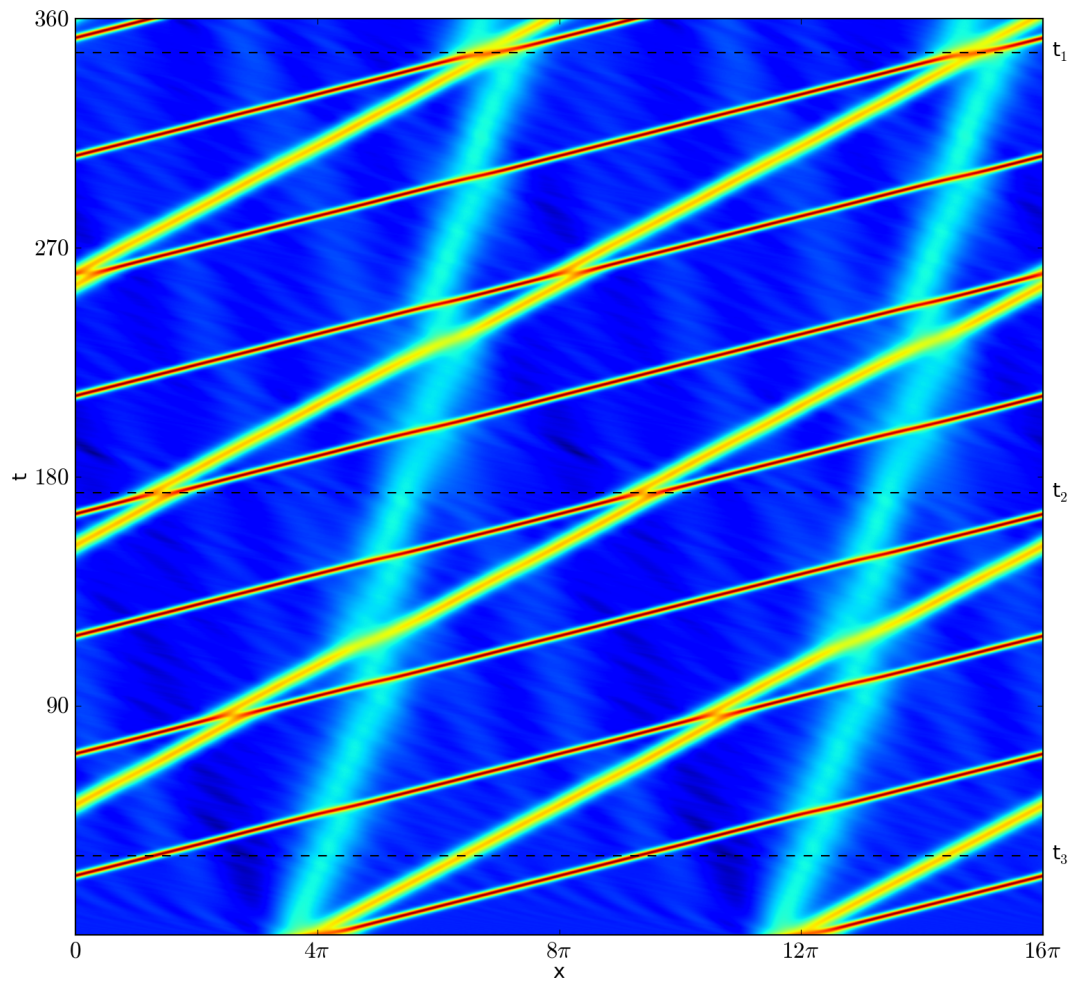


(b) Pseudocolor plot

Figure 14: Solution of cn^2 IC where $P = 2\pi$, $A = 5$, $\alpha_1 = 0.4$, $\alpha_2 = 0.028$



(a) Spectral amplitudes



(b) Pseudocolor plot

Figure 15: Lengthened cn^2 IC where $P = 8\pi$, $A = 1$, $\alpha_1 = 0.4$, $\alpha_2 = 0.028$

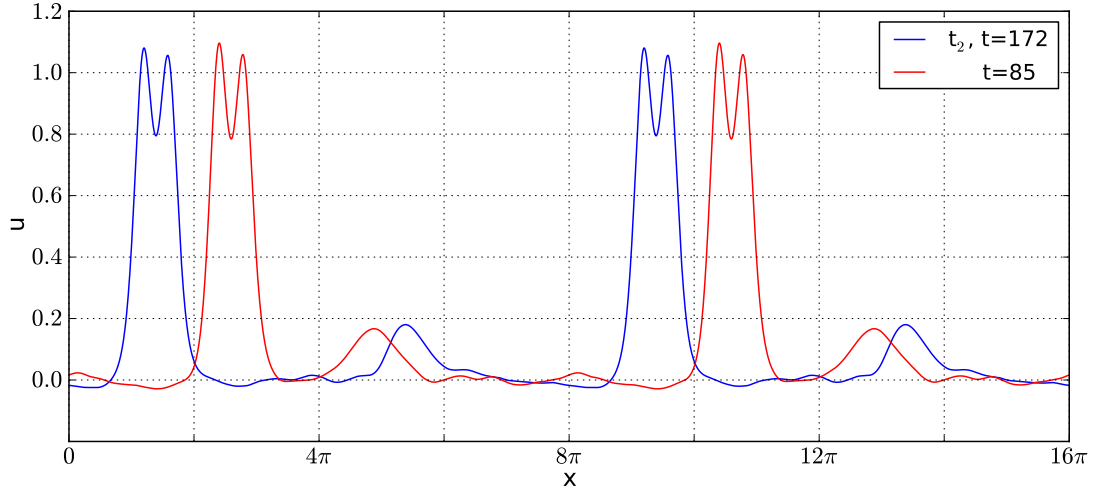


Figure 16: Slices of Fig. 15(b) where 1st and 2nd solitons interact. Depending on the distance between the interaction point and the 3rd soliton, the spectral amplitudes (Fig. 15(a)) can be very different. Lengthened cn^2 IC where $P = 8\pi$, $A = 1$, $\alpha_1 = 0.4$, $\alpha_2 = 0.028$

7.2 The influence of the microstructural dispersion parameter α_2

In this subsection, the effect of the parameter α_2 is considered in both the low m and high m cases. For doing so, the parameter α_1 is fixed to $\alpha_1 = 0.4$ and amplitudes $A = 1$ (Table 2) and $A = 5$ (Table 3) are used.

Table 2: Number of visible solitons with number of hidden solitons in parentheses; $A = 1$, $\alpha_1 = 0.4$, and $m = 0.5628$.

α_2	α_1/α_2 ratio	cn^2 & 2π		cn^2 & 8π		sech^2 & 8π	
		No. sol-s	SA fit	No. sol-s	SA fit	No. sol-s	SA fit
0.004	100	6(+2)	All	8 + t.	a_4	11(+1)	a_5
0.0055	72.7	6(+1)	All	7 + t.	a_4	9(+2)	a_4
0.016	25.0	4(+1)	All	4 + t.	a_2, a_3	6	a_3
0.017	23.5	4	All	4 + s.t.	a_2	6	a_3
0.028	14.3	3(+1)	All	3 + t.	a_2	5	a_2

The effect of the α_2 parameter remains the same regardless of the shape of the IC (indicated by parameter m and here changed by amplitude A). This confirms the results from Sec. 6.4, where was demonstrated that the number of solitons depends on the ratio α_1/α_2 . From Tables 2 and 3 can be seen that the number of solitons, including hidden

Table 3: Number of visible solitons with number of hidden solitons in parentheses. $A = 5$, $\alpha_1 = 0.4$, and $m = 0.9751$.

α_2	α_1/α_2 ratio	cn^2 & 2π		cn^2 & 8π		sech^2 & 8π	
		No. sol-s	SA fit	No. sol-s	SA fit	No. sol-s	SA fit
0.004	100	9(+4)	a_5	13(+1)	a_4, a_5	12(+1)+w.t.	a_4, a_5
0.0055	72.7	8(+3)	a_4	11+w.t.	a_4	11(+1)+w.t.	a_4
0.016	25.0	5(+1)	a_3	6+w.t.	a_3	6(+1)	a_3
0.017	23.5	5(+1)	a_3	6+w.t.	a_3	6+t.	a_3
0.028	14.3	4(+1)	a_2	5+w.t.	a_2	5	a_2

solitons, decrease as the parameter α_2 increases.

The number of solitons emerging from $P = 2\pi$ cnoidal and $P = 8\pi$ lengthened cn^2 -shaped initial waves increase when the amplitude A increases from $A = 1$ to $A = 5$. The total number of solitons remain comparable between the results of $P = 2\pi$ cnoidal and $P = 8\pi$ lengthened cn^2 -shaped ICs. However this comparison is slightly better in case of $A = 5$ than for $A = 1$. Solutions from sech^2 -shaped initial wave are less affected by this change of amplitude.

The results from $P = 8\pi$ lengthened cn^2 -shaped initial wave have tail for all results. The tail weakens as the amplitude increases. This can be attributed to the initial profile being smoother and mimicking the sech^2 -shaped initial profile more closely. As the $P = 2\pi$ cnoidal and $P = 8\pi$ sech^2 -shaped ICs satisfy the macrostructure KdV ($\psi_1 = 0$), they produce little or no tail.

7.3 The influence of the change of the macrostructural dispersion parameter α_1 and amplitude A

In this subsection, the effect of the change of the α_1 and A is studied while keeping the parameter m and thus the shape of the IC constant. In the present study, it has been found that the parameter m can be kept constant for Eqs. (6) and (5) with the relation

$$m \sim \frac{A}{\alpha_1} \left(\frac{P}{\pi} \right)^2. \quad (17)$$

The parameter m and the ratio of α_1/α_2 has been fixed. Here the shape of the initial wave has been kept constant by fixing the parameter $m = 0.9530$ with Eq. (17). Moreover, the ratio of α_1/α_2 is here also fixed, because as confirmed in a previous subsection, this ratio influences the number of emerging solitons. From Table 4 can be seen that the results are practically identical with the number of solitons, hidden solitons and the existence of tail remaining constant. In Fig. 17 can be seen that the results are actually identical. Moreover, waves coincide completely when the wave profile is normalized by the IC amplitude (Fig. 18). This also leads to the propagation times normalizing the same way, as the solitons' speed depends on their amplitudes. The same coincidence is attainable by changing the period length P instead of parameter α_1 or amplitude A to keep m constant (Eq. (17)).

This result corroborates Ilison's statement that with sech^2 IC under HKdV, the change of amplitude does not affect the solution [5] (for then all $m \approx 1$).

In other words, to keep the resulting wave field constant, the shape of the cnoidal IC, here given by parameter m , and the micro- to macrostructural dispersion ratio needs to be kept constant. The parameter m can be kept constant with Eq. (17). Increasing the α_1/α_2 ratio increases the number of visible and hidden solitons formed. In the future analysis, the IC amplitude A and macrostructural dispersion α_1 can be dropped from the parameter space and only the parameter m and ratio α_1/α_2 analysed. Since the wave field depends on these two values, the analysis of hidden solitons also should concentrate on the shape properties of the IC and the ratio of dispersion parameters for HKdV.

Table 4: Results where $m = 0.9530$

A	α_1	$\frac{\alpha_1}{\alpha_2}$	α_2	cn ² & 2π		cn ² & 8π		sech ² & 8π	
				No. sol.-s	SA fit	No. sol.-s	SA fit	No. sol.-s	SA fit
4.0	0.4	72.7	0.00550	8(+2)	a_4	10+t.	a_4	10(+1)-	a_4
		25.0	0.01600	5(+1)	a_3	6+t.	a_3	6(+1)	a_3
		14.3	0.02800	4(+1)	a_2	5+t.	a_2	5	a_2
3.0	0.3	72.7	0.00413	8(+2)	a_4	10+t.	a_4	10(+1)-	a_4
		25.0	0.01200	5(+1)	a_3	6+t.	a_3	6(+1)	a_3
		14.3	0.02100	4(+1)	a_2	5+t.	a_2	5	a_2
1.0	0.1	72.7	0.00138	8(+2)	a_4	10+t.	a_4	10(+1)-	a_4
		25.0	0.00400	5(+1)	a_3	6+t.	a_3	6(+1)	a_3
		14.3	0.00700	4(+1)	a_2	5+t.	a_2	5	a_2

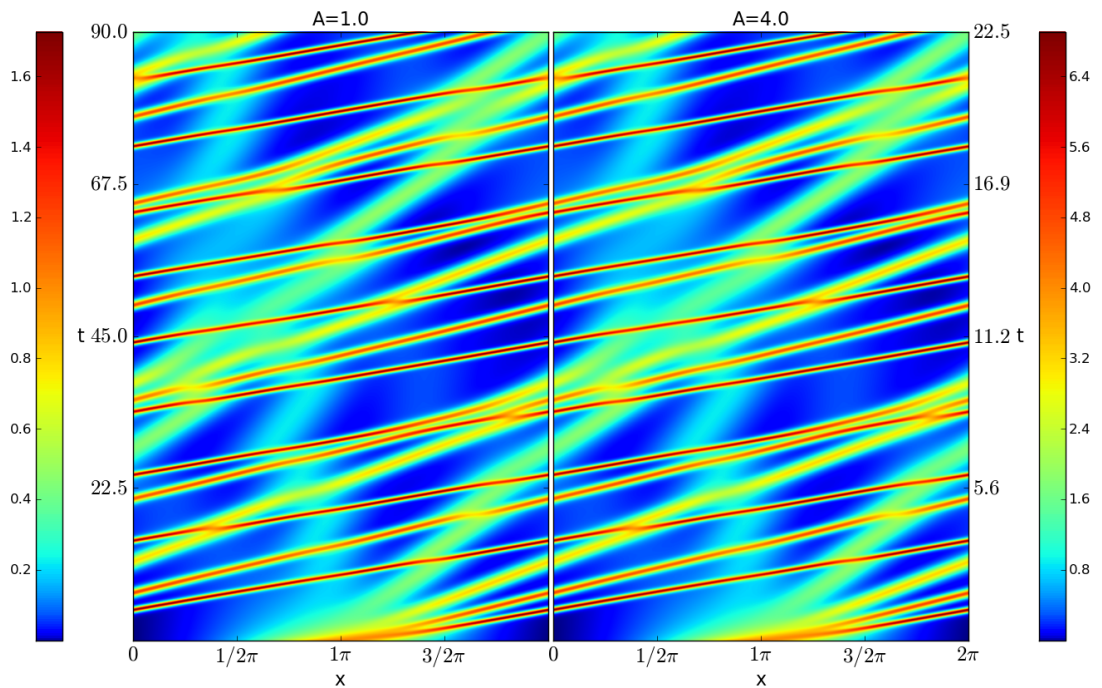


Figure 17: Pseudocolor plots ($m = 0.9530$, $\alpha_1/\alpha_2 = 25$)

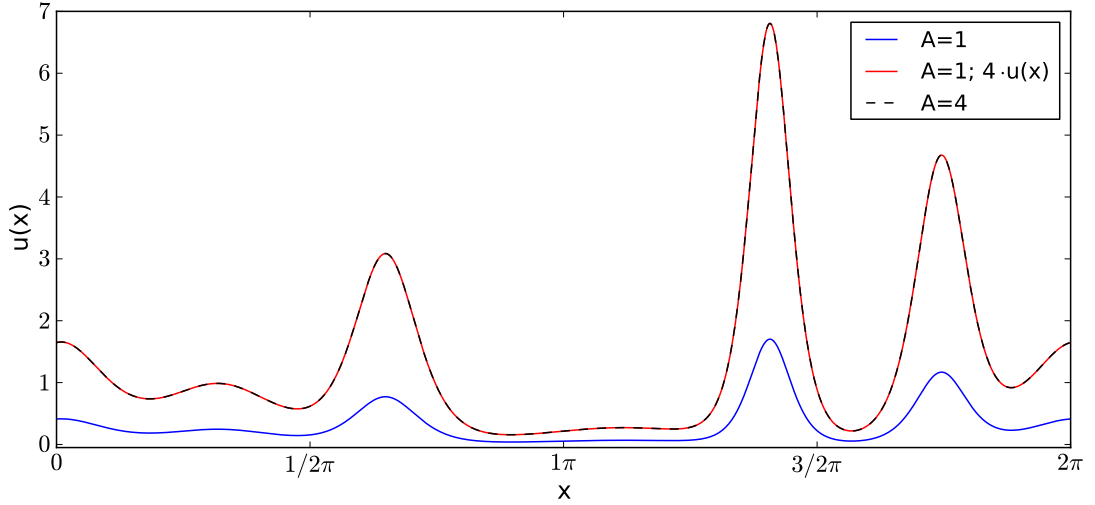


Figure 18: Final profiles of Fig. 17

Conclusions

This study has addressed the questions of whether the hidden solitons emerge in HKdV, under which ICs they emerge and what methods could be used for detecting them. This is important in theoretical treatises and practical measurements, because hidden solitons carry energy and influence other emerging waves. As the number of hidden solitons depends on the total number of solitons and the influence of the tail, these aspects have also been briefly investigated.

Firstly, solutions were computed using a pseudospectral collocation method. It was found that with high spatial resolution and high order of differentiation, the pseudospectral method's accuracy depends on the smoothness of emerging wave profiles and the numerical precision of the computer. It was found that for this work, filtering of the Fourier modes is necessary to keep the solution from exceeding the computer's numerical resolution and a relation found for setting the filtering parameters for use with pseudospectral method.

Secondly the $\alpha_1 - \alpha_2$ dispersion parameters of the HKdV were scanned using sech^2 -shaped initial wave. For the cases considered, it was found possible to minimize the emergence of the tail in the solution. This can be done by careful selection of the ratio of α_1/α_2 . The total number of emerging solitons also depends on this ratio.

For the main results of this thesis it was found that the hidden solitons do emerge in HKdV system under the three kinds of ICs considered: the cnoidal wave with a period of $P = 2\pi$, the sech^2 -shaped wave with a period of $P = 8\pi$ (Tables 1–4) and the cnoidal wave which was padded with zeros and lengthened to $P = 8\pi$ (Table 3). The number of hidden solitons depend on the total number of emerging solitons. If the number of emerging solitons increases while the spatial period remains the same, more solitons will stay hidden. Although, initially the long-period results were computed for verification purposes, it was found that the number of solitons emerging from the $P = 2\pi$ cnoidal and $P = 8\pi$ lengthened cn^2 results are not identical but merely comparable. The $P = 2\pi$ results can actually have more emerging solitons (when including hidden ones) than the $P = 8\pi$ results with the same equation parameters. Therefore the long-period results cannot be used as the only detection tool for hidden solitons in short-period results.

It is known that hidden solitons become visible after many interactions and are sometimes only detectable from their influence on the higher solitons when no other solitons are nearby. The interactions are best seen from the maxima curves, which show the amplitudes of the emerged solitons through time. In case of the nearly harmonic IC, the peaks of the spectral amplitudes of the solution point to the interactions between the solitons, and therefore also the hidden solitons as in [6]. It was found that it is difficult to use this method in case of nonharmonic initial waves and it requires locating a sufficient recurrence. The spectral data then points to some more characteristic interactions between the solitons.

The various ICs used in this work demonstrated that if the shape of the IC does not suit the KdV operator well, the tail will emerge. For more suitable ICs the tail also depends on the ratio of the micro- and macrostructure parameters. It was shown that in the parameter space, ratios exist along which the solution exhibits a smaller or no tail, probably due to some sort of agreement between the micro- and macrostructure. The formation of the tail has also been briefly investigated.

Finally, the effect of the shape of the initial cnoidal wave, characterised by the elliptic parameter m , was found to be significant to the results. It changes the soliton propagation lines, affecting the DSA, as mentioned above. It was found that if the parameter m and the ratio of α_1/α_2 are kept constant then identical wave profiles are formed. These wave profiles can be normalized in amplitude and time by the amplitudes of their initial

cnoidal waves. A simple relation (17) was found which aids in keeping the parameter m constant while changing the macrostructural dispersion parameter α_1 , amplitude of the initial cnoidal wave A and its spatial period P accordingly.

The main goals of this thesis have been achieved. All in all, the hidden solitons were successfully generated in the HKdV under three different kinds of initial waves with many different shapes with the cnoidal shape being very suitable for the problem at hand. The detection of the hidden solitons is based on its interactions. Interactions can be detected from maxima curves or by DSA, but the DSA is presently suitable for detection only if the initial wave is harmonic or nearly so. Additionally, the relations for minimising the emerging tail and narrowing the parameter space have been found. Also, new insights have been found for the filtering of Fourier pseudospectral method in case of high order of derivatives and high spatial resolution.

Further studies would be needed to determine how DSA methods could be used in case of nonharmonic initial waves. Also, other indicators of DSA, like cumulative spectrum or time averaged normalised spectral densities, might be used to analyse the solution. In the future, the initial conditions could also be further generalised.

Resüme

Käesolevas töös uuritakse peidetud solitonide formeerumist ja tuvastamist hierarhiliises Kortewegi-de Vriesi süsteemis. Solitonide füüsika jaoks on põhjanevaks saanud Kortewegi ja de Vriesi 1895. a artikkel [1] madalas vees levivatest mittelineaarsetest pikkadest lainetest. Sellest kujumuutuseta levivate veelainete uurimusest on tänapäevaks välja kasvanud füüsikaharu, mis hõlmab muuhulgas hüdrodünaamilisi laineid, plasmalaineid, informatsiooni levikut ülekandeliinides ja optilistes kaablites ning lainelevi granuleeritud materjalides. Solitone käsitletakse antud töös kui stabiilseid, kellekujulisi laineid, mis levivad konstantse kiiruse ja amplituudiga [7]. Peidetuteks nimetatakse selliseid solitone, mida pole näha algsest solitonide jadast [2].

Hierarhiline Kortewegi-de Vriesi võrrand (HKdV) on tuletatud Giovine ja Oliveri poolt lainelevi modelleerimiseks granuleeritud materjalides [4]. Mudelvõrrand on lahendatud perioodiliste rajatingimustega ja kolme tüüpi algtingimuse jaoks: (i) Jacobi cn^2 -kujuline (noidaalne) laine (6); (ii) “pikendatud” Jacobi cn^2 -kujuline laine (8); (iii) $sech^2$ -kujuline laine (7). Antud viiendat järku segaosatuletistega mittelineaarne diferentsiaalvõrrand on lahendatud pseudospektraalmeetodiga.

Käesoleva töö tulemused näitavad, et HKdV võrrandi lahendis võib esineda peidetud solitone. Need tekivad lihtsamini lühikese ruumiperioodiga algtingimustest ning juhtudel kui algtingimusest formeerub palju solitone. On leitud, et kõigi kolme vaaeldud algtingimuse puhul eksisteerivad parameetrid, millega tekib peidetud solitone (Tabelid 1–4).

Peidetud solitone saab tuvastada nende interaktsioonidest suurema amplituudiga solitonidega. Nende vastasmõju avaldub kõige selgemalt solitonide amplituudikõverate abil. Lokaalsed miinimumid või nõgusused neil kõverail osutavad interaktsioonidele väiksemate solitonidega [2]. Töös on uuritud ka interaktsioonikohtade leidmist diskreetse spektraalanalüüsi meetoditega [6]. Selgub, et need meetodid on kasutatavad ka HKdV puhul, kuid selleks peab algtingimus olema suhteliselt monokromaatiline. Üldisema kujuga algtingimuste lahendites ei näita spektraalandmed interaktsioone enam niivõrd üheselt.

Lisaks põhitulemustele on antud töös leitud ka seaduspärasus, millal hakkavad numbrilised vead pseudospektraalmeetodiga lahendamisel tekkima ja kuidas leida filtreeri-

miseks [6] tarvilikke lainearvude piire. Samuti on tuvastatud, et HKdV mudelil leiduvad kindlad dispersiooniparameetrite suhted, mille puhul lahendis tekkiv “saba” on minimaalne. Veelgi enam, osutub, et sellest suhtest sõltub tekkivate solitonide arv. Edasi on näidatud, et dispersiooniparameetrite suhte ja algingimuse kuju fikseerimisel jääb HKdV lahend pärast alglaone amplituudiga normeerimist samaks (Joon. 17). On ka leitud lihtne seos (17) laine amplituudi, perioodi ja dispersiooniparameetri vahel, mille abil saab noidaalse laine kuju fikseerida. Osutub, et noidaalne laine on väga sobilik HKdV võrrandiga peidetud solitonide uurimiseks.

Käesoleva töö esialgsed tulemused on ette kantud IMACS rahvusvahelisel konverentsil [7].

Acknowledgments

My deepest gratitude goes to my supervisor Prof. Andrus Salupere, for his friendly guidance on all aspects of this academic work. I would also like to thank my beloved Pille for her support and encouragement during the writing of this thesis. Financial support from Estonian Science Foundation Grant No. 8658 is greatly appreciated.

References

- [1] D. J. Korteweg, G. de Vries, On the change of form of long waves advancing in a rectangular canal, and on a new type of long stationary waves, *Phil. Mag.* 39 (1895) 422–443.
- [2] A. Salupere, G. A. Maugin, J. Engelbrecht, Korteweg–de Vries soliton detection from a harmonic input, *Phys. Lett. A* 192 (1) (1994) 5–8.
- [3] J. Engelbrecht, A. Salupere, On the problem of periodicity and hidden solitons for the KdV model, *Chaos* 15 (2005) 015114.
- [4] P. Giovine, F. Oliveri, Dynamics and Wave Propagation in Dilatant Granular Materials, *Meccanica* 30 (4) (1995) 341–357.
- [5] L. Ilison, Solitons and solitary waves in hierarchical Korteweg–de Vries type systems, Ph.D. thesis, Tallinn University of Technology (2009).
- [6] A. Salupere, The pseudospectral method and discrete spectral analysis, in: E. Quak, T. Soomere (Eds.), *Applied Wave Mathematics: Selected Topics in Solids, Fluids, and Mathematical Methods*, Springer, Berlin, 2009, pp. 301–333.
- [7] A. Salupere, M. Lints, On existence of hidden solitons in solitonic structures, *The Eight IMACS International Conference on Nonlinear Evolution Equations and Wave Phenomena: Computation and Theory*, March 25–28, 2013 (2013).
- [8] A. Salupere, G. A. Maugin, J. Engelbrecht, J. Kalda, On the KdV soliton formation and discrete spectral analysis, *Wave Motion* 23 (1) (1996) 49–66.
- [9] I. Christov, Hidden solitons in the Zabusky–Kruskal experiment: Analysis using the periodic, inverse scattering transform, *Math. Comput. Simulat.* 82 (6) (2012) 1069–1078.
- [10] P. L. Bhatnagar, *Nonlinear waves in one-dimensional dispersive systems*, Oxford University Press, 1979.
- [11] G. A. Korn, T. M. Korn, *Mathematical handbook for scientists and engineers*, Dover publications, Inc., 2000.

- [12] S. Adlaj, An eloquent formula for the perimeter of an ellipse, *Notices of the AMS* 59 (8) (2012) 1094–1099.
- [13] N. J. Zabusky, M. D. Kruskal, Interaction of solitons in a collisionless plasma and the recurrence of initial states, *Phys. Rev. Lett.* 15 (1965) 240–243.
- [14] B. Fornberg, *A Practical Guide to Pseudospectral Methods*, Cambridge University Press, Cambridge, 1996.
- [15] M. Frigo, S. Johnson, The design and implementation of FFTW3, *Proceedings of the IEEE* 93 (2) (2005) 216–231.
- [16] K. Radhakrishnan, A. C. Hindmarsh, Description and use of LSODE, the livermore solver for ordinary differential equations, Tech. rep., Lawrence Livermore National Laboratory, UCRL-ID-113855 (1993).
- [17] P. Peterson, F2PY: a tool for connecting Fortran and Python programs, *Int. J. Computational Science and Engineering* 4 (4) (2009) 296–305.
- [18] E. Oran Brigham, *The Fast Fourier Transform and Its Applications*, Prentice Hall Int., London, 1988.
- [19] E. Jones, T. Oliphant, P. Peterson, *SciPy: open source scientific tools for Python*, (2007), URL <http://www.scipy.org>.
- [20] Enthought tool suite, URL <http://code.enthought.com/projects/>.

A Example: FFT of $\sin(x)$ where $x \in [0, 2\pi)$

The range of x is discretized with 2048 points, which should give a good approximation to the continuous case. Fourier transform of a sine should give k_1 and k_{-1} as the only nonzero wavenumbers. If the plot is zoomed in (Fig. 19), it is apparent that the supposed “zero” instead oscillates between machine epsilon ($\sim 10^{-16}$) and $\sim 10^{-14}$. Here no magnitudes are actually zero. This is natural and expected.

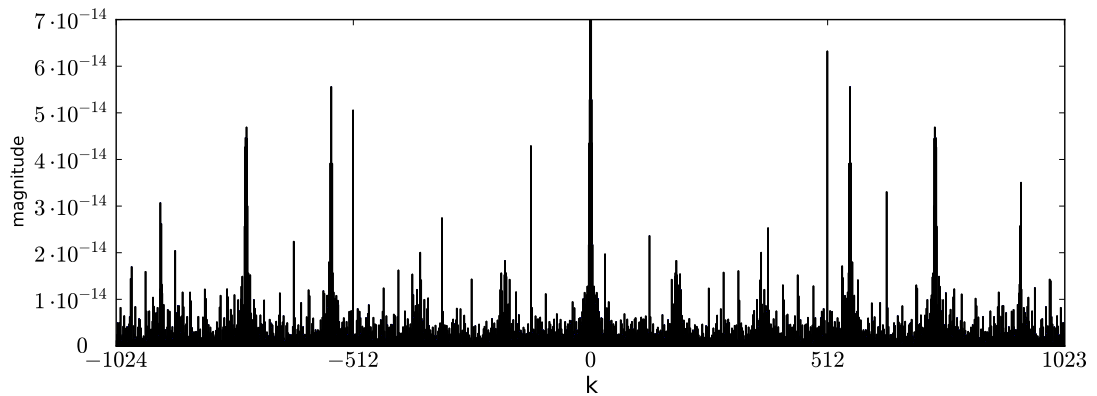


Figure 19: Magnitude of complex wavenumbers $F \sin(x)$ with 2048 points

Even though this kind of precision seems enough for most cases, sometimes high spatial derivatives of datasets with thousands of space-grid points need to be taken. From Eq. (12), this leads to multiplication with a very high wavenumber taken to the power of the desired derivative order. If, in this example, 5th derivative of the sine is taken using pseudospectral method, the highest wavenumber in the power of 5 would be $1024^5 = 1.12 \cdot 10^{15}$ which will bring numerical error oscillations to the visible range (Fig. 20). After that, no further meaningful derivatives can be taken (Fig. 21).

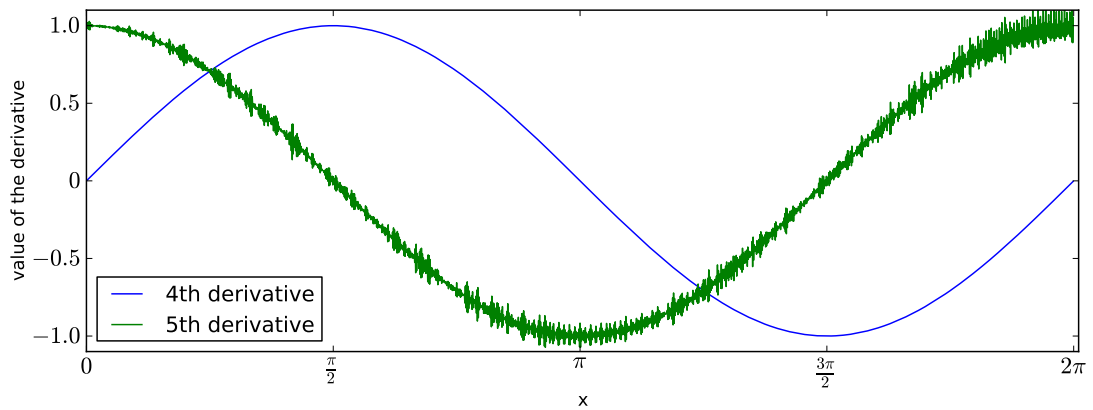


Figure 20: 4th and 5th derivatives of $\sin(x)$

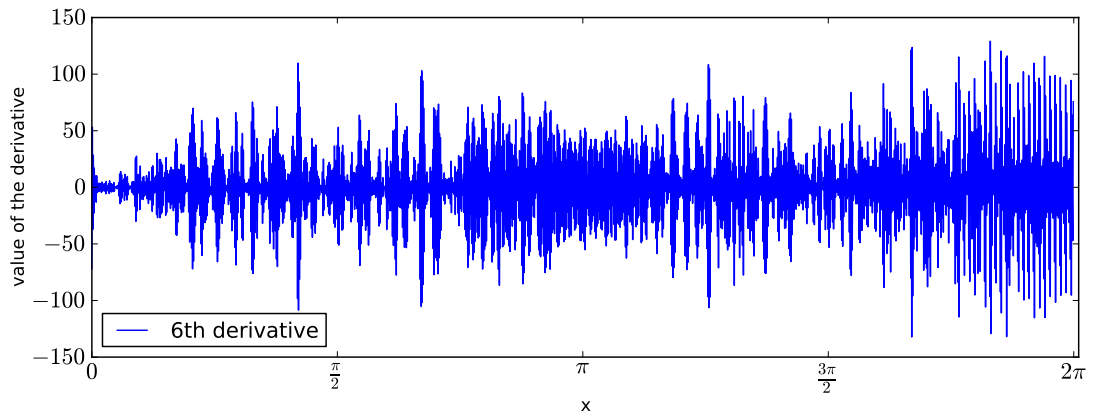


Figure 21: 6th derivative of $\sin(x)$, which is unusable

In order to get accurate results, the Fourier components must tend to zero if $|k| \rightarrow N/2$ [6]. As a result the high wavenumber modes do not carry any significant energy and can be filtered out. The maximum nonzero or unfiltered k can be worked out depending on the FFT's and the computer's precision and the order of differentiation. Figure 22 displays the lines for 3rd, 4th and 5th derivative where the unfiltered k would be the same magnitude as the available numerical precision. In filtering the information is only lost if the filtered modes (high wavenumber modes) carry necessary information (energy). A wave profile does not contain energy in high wavenumber modes if it is smooth and has no discontinuities.

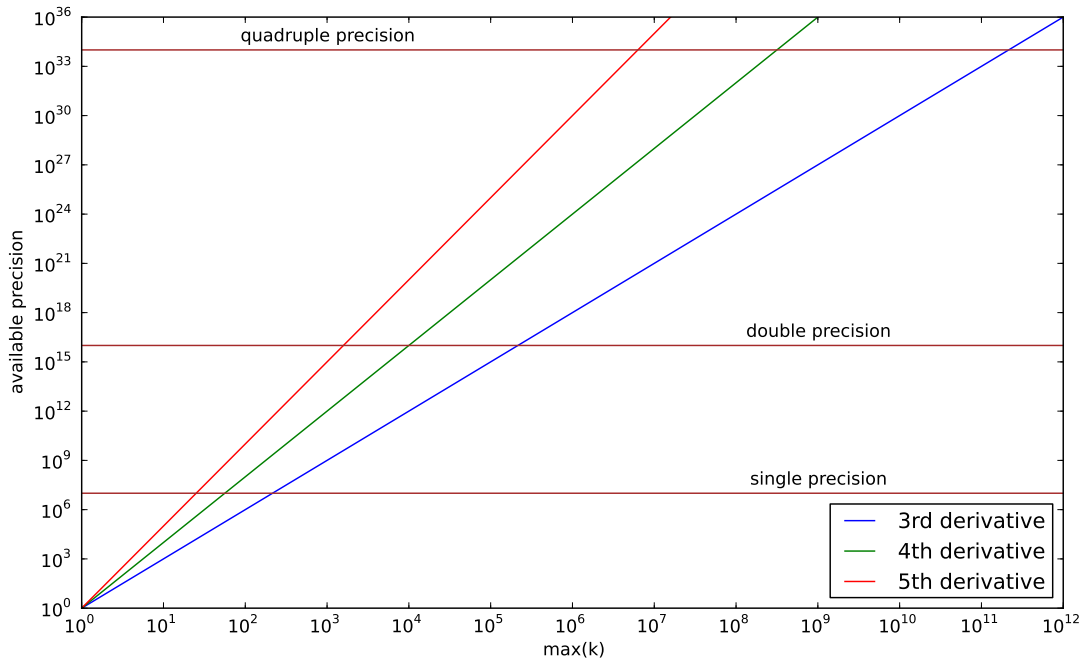


Figure 22: Lines where differentiation fills all available precision

The sine taken in this example has only the first wavenumber (k_1 and k_{-1}) mode as nonzero and the same goes for its derivatives, so all the higher wavenumber modes, which could potentially bring out the numerical oscillations can be zeroed without any information lost. Generally the wave profile is more complex and more modes will be needed but usually, when analysing wave profiles, the highest modes can be filtered out, allowing for extra spatial resolution or higher derivatives.